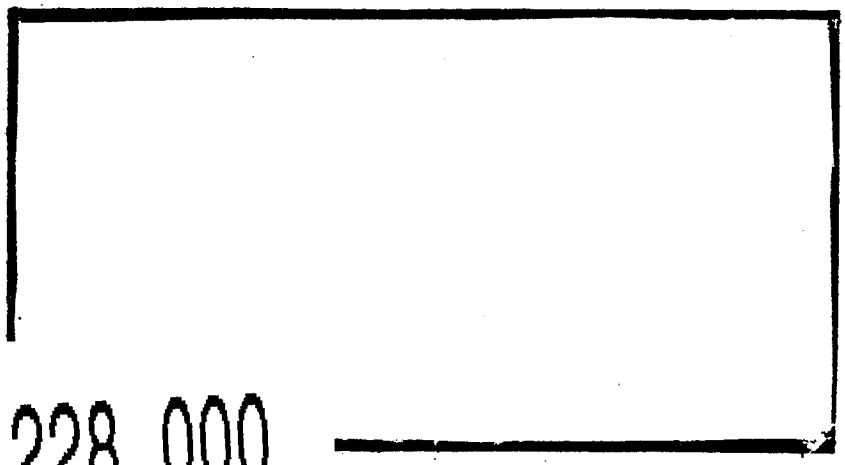

DEPARTMENT OF THE AIR FORCE

AIR UNIVERSITY

AIR FORCE INSTITUTE OF TECHNOLOGY

Wright-Patterson Air Force Base, Ohio

AFIT/GAP/ENP/94D-05

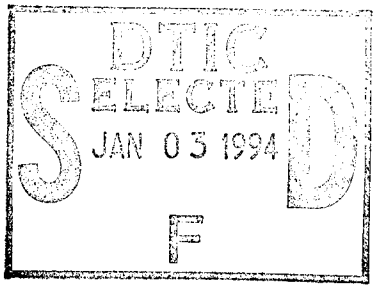

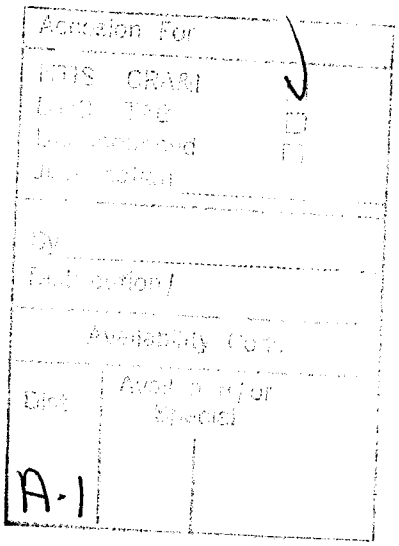

DETECTING ALPHA PARTICLES THROUGH SCINTILLATION IN POROUS MATERIALS

THESIS

Martin E. Keillor, Captain, USAF

AFIT/GAP/ENP/94D-05

Approved for public release; distribution unlimited

The views expressed in this thesis are those of the author and do not reflect the official policy or position of the Department of Defense or the United States Government.

AFIT/GAP/ENP/94D-05

DETECTING ALPHA PARTICLES THROUGH SCINTILLATION IN POROUS MATERIALS

THESIS

Presented to the Faculty of the Graduate School of Engineering

of the Air Force Institute of Technology

Air University

In Partial Fulfillment of the

Requirements for the Degree of

Master of Science

Martin E. Keillor, B. S.

Captain, USAF

December, 1994

Acknowledgments

I take this opportunity to thank a multitude of people who assisted me in accomplishing this thesis. First and foremost, I thank Dr. L. W. Burggraf for recruiting me to pursue one of his ideas for the use of gel-silica in alpha particle detection. Without his concepts and guidance I would not have undertaken nor completed this project. I am also indebted to Dr. Harley Ross for providing me computer code which proved an excellent starting point for the modeling presented herein. Samples of gel-silica sent by Dr. Jon West were crucial, not only to the experimental work but to the project as a whole. Dr. Harvey Paige also supplied laboratory materials which were unavailable in the AFIT labs. Key suggestions came from Dr. G. John, Dr. D. Weeks, and Captain J. Martin. Technician Leroy Cannon gave invaluable assistance in the laboratory, and I am especially grateful to Bob Hendricks for coming in on his own (retirement) time to get me started in the lab. Finally, I thank my wife, Katy, and family for putting up with my surly demeanor during this work, and for sacrificing the entire dining room table to my papers for months.

Martin E. Keillor

Table of Contents

Page

Page

List of Figures

Figure Page

List of Tables

Abstract

This thesis presents the results of a preliminary study of some of the parameters essential to the development of a scintillation flow-cell detector with improved characteristics over existing cells. Such a detector with better than 10% alpha energy resolution could provide *in situ* capability to detect and identify important alpha-emitting radionuclides in dilute aqueous solutions. Gel-silica is a potential candidate that may provide the needed improvement in resolution while maintaining 100% detection efficiency; however, gel-silica with useful light output is yet to be developed. As a step toward realizing the system described, the dependence of alpha detection efficiency and intrinsic energy resolution on the phase dimensions in heterogeneous scintillation detectors is examined. Two main areas of this research are: 1) computer modeling of the geometric detection efficiency and intrinsic energy resolution in particulate and porous glass scintillation detectors, and 2) experiments designed to test model predictions and to provide data on the detection of alphas in porous glass structures. Experimental emphasis is on alpha detection in gel-silica filled with liquid scintillant. Results show that phase dimensions must be considered in constructing a flow-cell detector for alpha spectroscopy, and that the dimensions available in gel-silica provide for excellent intrinsic energy resolution, as well as 100% detection efficiency.

DETECTING ALPHA PARTICLES

THROUGH

SCINTILLATION IN POROUS MATERIALS

I. Introduction

The advent of a system capable of *in situ* determination of the isotopic concentrations of alpha emitting nuclides dissolved in water would be a significant improvement over methods currently used to detect and identify these radionuclides. Alpha, gamma, and x-ray emissions from such nuclides are the main candidates for fingerprinting specific isotopes and allowing determination of their concentrations in an *in situ* detector. The motivations for seeking such a system include a variety of potential applications which require monitoring alpha emitters in environmental waters. Elevated concentrations of naturally-occurring alpha emitters, (particularly radium, ^{222}Rn, and uranium) have been found in water supplies across the United States (Blanchard *et al*, 588: 1985). The population drinking from such contaminated water supplies face a health risk associated with the intake of alpha emitters. Radionuclides associated with man's activities in the nuclear realm pose a similar threat if allowed to contaminate surface or ground water in the vicinity of a nuclear facility. Additionally, such man-made isotopes are a valuable source of information on the status of countries suspected of nuclear

proliferation activities. The current and future need for knowledge of alpha activity contained in environmental water, along with the current costs for obtaining such information, makes the development of an *in situ* alpha detector a worthy goal.

Current methods used to quantify isotopic concentrations of alpha emitting nuclides in water generally involve chemical separation methods which are time consuming and costly. Typical methods involve liquid-liquid extraction (McDowell and McDowell, 115: 1991), coprecipitation (McCurdy and Mellor, 250: 1981), or other laboratory techniques designed to isolate the element of interest prior to radiation measurement. Although methods for field determination of the gross alpha activity in water samples are available (Blanchard *et al*, 590: 1985), a portable system capable of simultaneously determining the activities of several nuclides in a low activity, mixed sample is not available. Such a system is the goal of a project recently initiated at the Air Force Institute of Technology (AFIT) by Dr. Larry Burggraf.

One system design being considered for this project uses a heterogeneous scintillation flow cell detector, operated in coincidence mode with a gamma or other suitable detector. The intent is to identify alpha emitters based on their alpha energies, or at a minimum associate alpha emitters into sufficiently small groups via alpha spectroscopy so that further identification can be accomplished based on coincident radiations. Unfortunately, alpha spectroscopy is generally not accomplished with flow cell detectors because of their poor energy resolution capabilities. To overcome this problem, the possibility of constructing a flow cell from porous glass is being considered. Gel-silica is a porous silica glass which offers phase dimensions on the order of nanometers and less

which may allow improvements in alpha energy resolution by offering less self-absorption of scintillation light and better intrinsic energy resolution capabilities than are available in current heterogeneous scintillation detectors.

Problem and Scope

This thesis is a step toward realization of the detection system just described. The problem examined here is the dependence of geometric efficiency and intrinsic energy resolution on the dimension of phase regions in heterogeneous scintillation detectors used for detecting alpha particles. Emphasis of this research was divided into two main areas: 1) computer modeling of the geometric detection efficiency and intrinsic energy resolution in particulate and porous glass scintillation detectors, and 2) experiments designed to test several of the model predictions and provide data on the detection of alphas in porous glass structures. A large portion of the experimental work concentrated on alpha detection in gel-silica, which is a new application of this recently developed material.

Sequence of Presentation

Chapter 2 of this paper provides background material intended to inform the reader of detection methods and requirements which motivated the current research. Computer modeling and the results of that modeling are discussed in Chapter 3, followed by experimental results in Chapter 4. Results of this research and recommendations for further work are presented in the final chapter.

II. Background

Flow cell detectors are currently used to monitor nuclear radiations in a variety of applications. Unfortunately, current heterogeneous flow cell detectors suffer reductions in both detection efficiency and energy resolution capability due to alpha energy loss in the inactive phase of the detector. These reductions are further compounded by self absorption of scintillation light common to such detectors. This chapter presents background material on current uses of flow cell detectors, followed by several flow cell concepts which may be applicable to the project described in the introduction. Gel-silica glass is introduced as a possible flow cell component, and its physical properties are discussed. Finally, resolution and efficiency requirements necessary to successfully detect and differentiate alpha emitting nuclides are covered.

Flow Cell Scintillation Detectors.

Burggraf has proposed that a flow cell scintillation detector, operated in coincidence mode with a suitable gamma or other detector, may provide an in-situ capability to quantify and distinguish alpha emitters with little or no advance separation of elements (Burggraf: 1994). Homogeneous and heterogeneous scintillation cells have been reported in the literature, both of which are designed to place the sample in close proximity to the scintillation material. In a homogeneous cell, liquid scintillation cocktail is mixed with a liquid sample prior to entering the counting chamber. Heterogeneous cells

pass a liquid or gaseous sample through a porous scintillation material, often powdered crystalline scintillators, plastic scintillator spheres, or bundled scintillating fibers.

Flow cell detectors are used to detect alpha and beta particles in a variety of applications, including liquid chromatography detectors, in-line process monitors, and environmental measurement and control devices (Ross, 195: 1991). These applications are generally limited to counting work, with alpha spectroscopy beyond the realm of flow cells due to their poor energy resolution capability. Porous gel-silica glass offers light transmission characteristics which should improve energy resolution over that available from current flow cell designs.

Traditional flow cell detectors do not preconcentrate radionuclides prior to counting, allowing operation in near real time without suffering ever-increasing detection limits due to an increasing background of adsorbed radionuclides. The use of porous gel-silica as a flow cell is likely to result in a high rate of adsorption of some radionuclides because of the high surface area contained in the gel-silica pore structure. Although this feature may seem inconvenient since increases in background would occur, it may actually allow reductions in detection limits by allowing the concentration of nuclides of interest (Burggraf: 1994). This improvement would be gained at the expense of detector response time, as time for the collection cycle may be required.

Gel-silica. Ross lamented:

> It also appears that using conventional powdered materials for the solid scintillator cell phase cannot improve detector geometry and reduce photon scatter simultaneously. This apparent stalemate is unfortunate since improved flow cell detectors would have a broad range of important applications. (Ross, 197: 1991)

Using porous gel-silica glass in place of particulate scintillators may break this stalemate and allow excellent counting efficiency combined with good light collection characteristics. Gel-silica is high purity SiO_2 glass formed through a low temperature chemical sol-gel process. This porous glass is produced through the creation of a hydrolyzed silica sol (dispersion of colloids in a solvent), followed by chemical condensation of the silica to produce a solid gel, and subsequent dehydration and thermal stabilization of the gel (Hench et al, 77-78: 1988). Gel-silica has several properties which make it attractive as a potential flow cell detector.

Porosity. Porosity is the volume fraction of void space within a material. Gel-silica can be manufactured with a variety of porosities, ranging from 0% (fully dense vitreous silica glass) to 70% (Hench et al, 11: 1993) and higher. The porosity is a function of the pore size and the number of pores contained in a sample. The pore size distribution is mainly determined by the preparation method used to create a particular gel-silica, while the number of pores remaining is a function of the temperature used to stabilize the sample. Under proper drying and stabilization conditions the pores remain interconnected in the finished product, which allows fluid to flow through the glass matrix. Thus the interconnected porosity allows gel-silica to be considered as a potential flow cell detector.

Pore Size. The mean pore radius of gel-silica materials depends on the method of preparation. Samples used in the experimental portion of this study have a

mean radius of 2 nm, with a narrow distribution of pore sizes (Hench et al, Fig 4: 1993). Gel-silica with mean pore radii in the range of 1 nm to 10 nm are available.

Surface Area. The surface area of porous gel-silica is also a function of the stabilization temperature. The surface area of a sample decreases as a function of increasing stabilization temperature. For example, the samples used in this study contain 200 m^2/g of surface area after stabilization to 1000°C. The same material stabilized to 800°C contains 550 m^2/g of surface area (Hench et al, 6: 1993). The adsorption of radionuclides onto surfaces in a flow cell is a function of the surface area contained in the cell, so that high surface areas are desirable if the intention is to collect nuclides of interest within the cell.

Scintillation. A gel-silica scintillator with useful light output has not been reported. However, glass scintillators are well known. Cerium doped glasses yield the highest light output of known silicate glass scintillators, with some formulations reported to exhibit pulse heights as high as 14% of that of NaI(Tl). Useful energy resolutions have also been achieved, notably 8.7% in detecting the products of the $^6Li(n,\alpha)$ reaction in lithium doped, cerium activated glass (Birks, 556-560). Researchers at the University of Florida, led by Dr. Larry Hench and Dr. Jon West, are currently attempting to create scintillating Ce^{+3} doped gel-silica samples. An initial sample provided for this work was doped by infusion of a cerium solution into a gel-silica matrix. This sample became opaque when doped and did not scintillate. Current efforts are focused on doping the material by including cerium in the sol. The low temperature sol-gel process also allows

the possibility of incorporating organic fluors into gel-silica components (Nogues et al, 1159: 1988). Considering these facts, it seems likely that gel-silica scintillators with usable light output will be developed in the future.

Light Transmission. Porous gel-silica is currently manufactured as optical components which are transparent in the visible wavelengths. However, scattering of light within gel-silica is noticeable in samples with 4.5 nm pores, and increases with increasing pore size (Hench, et al, 9: 1993). Filling the pores with a liquid reduces the scattering observed in gel-silica.

Gel-silica exhibits increasing absorption in the ultraviolet (UV) region. Samples with 3 nm pores drop to 50% UV transmission at a wavelength of 346 nm, with a 1% UV cutoff at 221 nm (Hench, *et al*, 9: 1993). These UV transmission characteristics may be further degraded by the presence of cerium when a cerium activated gel-silica scintillator is developed. However, cerium doped glass with light output of 14% of the intensity of NaI(Tl) has been reported. This glass emits light in the wavelength range of 320 to 500 nm, with a peak at 390 nm. The absorption spectrum for this glass is confined below 355 nm, and peaks at 305 nm (Birks, 557: 1964). These data suggest that, despite some self absorption, good light output and transmission should be available from a cerium doped gel-silica. Further, incorporation of a wavelength shifter within the glass may improve the light output of such a detector.

Casting. The method used to produce gel-silica lends itself to precision casting of components into a variety of shapes. Thus design of a detector benefits from the availability of a wide variety of geometries.

Stability. Stability in water is a necessary trait for flow cell components which will be exposed to aqueous samples. Unfortunately, the gel-silica samples used in this study suffered stress cracking when exposed to water. Thus the samples studied would be unsuitable for use in flow cells. However, gel-silica monoliths which are stable to water diffusion are available (West et al, Table 1: 1994).

Operation Modes. As previously mentioned, flow cell detectors generally allow radionuclides to pass through the cell unhindered. This allows use of the cell without loss of capability over time, although cells with high surface area suffer from memory effects (increasing background due to adsorbed radioisotopes). Intentionally collecting isotopes of interest via adsorption on surfaces within the cell is possible. High collection efficiencies could be achieved for many alpha emitters, particularly as the surface area of the flow cell is increased. For example, trace amounts of dissolved polonium have a strong affinity for silica surfaces (Figgins, 19: 1961). It may be possible to selectively adsorb ions of interest by controlling the pH of the influent (Iler, 673: 1979), or by chemically modifying surfaces within a flow cell.

Disadvantages of adsorbing radionuclides within the flow cell may be more than compensated for by two advantages this method offers. The disadvantages include possible increased counting cycle times and increasing limits of detection due to increasing background counts (resulting in the requirement to clean the cell or use disposable cells). Advantages include:

1) Increased source count rate. With high collection efficiency, the detection limits improve because the collected sample will have a higher activity than is contained in the volume of water that fits within the pore space of the flow cell.

2) Cycled collection/count system. A system based on a cycled collection/measurement sequence becomes possible. After collection of a sample on the flow cell surfaces, liquid scintillator is backfilled into the flow cell and the sample is counted. This system would allow use of a non-scintillating material as the solid phase of the flow cell. Backfilling a scintillating flow cell with a liquid (or gas) scintillator is also an appealing possibility. Since both phases are active materials in this case, no energy degradation occurs from losses in the inactive phase of the flow cell.

Challenges in Alpha Detection.

Achieving good energy resolution and high counting efficiency are challenging and necessary goals in the successful characterization of alpha emitters dissolved in water.

Energy Resolution. Solid state detectors provide the energy resolution required to identify most alpha emitters based on their alpha energies, however an *in situ* arrangement of such a detector is difficult to devise (as evidenced by the lack of such a device). Scintillation detectors, on the other hand, achieve the poorest energy resolution of any commonly used detector, but lend themselves to *in situ* system designs. As an example, commercial liquid scintillation counters designed primarily for beta detection provide alpha energy resolution on the order of 10% - 20%. Using a method called Photo-Electron Rejecting Alpha Spectroscopy (PERALS), McDowell has reported alpha energy

resolutions as good as 5% in a liquid scintillation system optimized for alpha detection (McDowell, 650: 1975).

Achieving 10% energy resolution with a flow cell detector would provide useful separation among several alpha emitters likely to be found in water supplies at levels high enough to cause concern. Blanchard, et al, listed ^{224}Ra, ^{226}Ra, ^{222}Rn, ^{234}U, ^{235}U, and ^{238}U as "the only natural [alpha emitters] likely to be in public water supplies at concentrations that may be of health concern" (Blanchard, 588: 1985). At 10% energy resolution, the ^{238}U peak, the composite peak of ^{234}U and ^{226}Ra, and the composite peak of ^{222}Rn and ^{224}Ra would have enough separation to be distinguished from one another. Alphas from ^{235}U occur at four energies that lie between the peaks from ^{234}U and ^{238}U, and would typically be present at significantly lower activities than ^{234}U and ^{238}U. Thus, quantification of ^{235}U based on alpha spectroscopy would not be possible at 10% resolution. Fortunately, the 70% alpha-gamma coincidence yield of ^{235}U makes this nuclide a prime candidate for identification based on alpha-gamma coincidence. Significant separation of the ^{222}Rn and ^{224}Ra alpha peaks do not occur until an alpha energy resolution on the order of 3% is reached. Additionally, the primary ^{226}Ra and ^{234}U peaks unresolved because they are separated by less than 0.01 MeV. However, the 3.9% alpha-gamma coincidence yield of ^{224}Ra and the 3.28% yield of ^{226}Ra may allow quantification of the contributions of these nuclides to their composite alpha peaks. Based

on these considerations, an alpha-gamma coincidence detector with 10% or better alpha energy resolution would be a valuable development.

Energy resolution in scintillation detection systems is limited primarily by statistical variations in (1) emission of photons by the scintillator, (2) light collection, (3) quantum efficiency of the photocathode, and (4) the electron multiplication process within the photomultiplier (Birks, 152-153: 1964), however the intrinsic energy resolution of a heterogeneous detector can also impact the resolution achieved by the system. Partitioning of deposited energy between scintillating and non-scintillating phases of a heterogeneous detector is subject to a statistical spread which contributes to the energy line width recorded by a flow cell scintillation detector. This contribution can be thought of as the detector's intrinsic energy resolution, and places the ultimate limit on the energy resolution achievable in a flow cell detector of a given composition.

Detection Efficiency. The short range of alpha particles in condensed phase materials places stringent requirements on alpha detection systems in order to achieve reasonable detection efficiencies. For example, the range of a 5 MeV alpha in water is on the order of 35 μm. Such a short range necessitates quantitative transfer of the isotope to an appropriate substrate or medium (i.e. liquid scintillation cocktail), or intimate contact between the detector and a suitable volume of the contaminated water. High detection efficiencies are desirable because the counting time required to achieve a specified statistical accuracy depends on the detection efficiency. For instance, the total time required to measure low level activity within a specified error follows the proportionality (Knoll, 96: 1989):

$$\frac{1}{T} \propto \frac{S^2}{B} \qquad (2\text{-}1)$$

where T is the time required for background and source + background counts
S is the count rate due to the source
B is the count rate due to background

S represents the product of the decay rate and the absolute detection efficiency, hence the counting time required is inversely proportional to the square of the absolute detection efficiency, and the highest possible detection efficiency is desirable to reduce required counting times. In a heterogeneous scintillation detector, the maximum possible detection efficiency is limited by the geometric detection efficiency of the system (assuming no energy transfer between the phases of the detector). The geometric detection efficiency is determined by the fraction of alphas generated which contact the active phase of the detector.

The geometric detection efficiency and intrinsic energy resolution of a heterogeneous flow cell are determined by the dimensions of the sensitive and non-sensitive phase regions in the cell relative to the range of an alpha particle in the cell. The absolute detection efficiency and the energy resolution of a system can be dominated by the geometric and intrinsic capabilities of the detection cell, respectively. For this reason, a modeling effort which examines the dependence of these properties on phase region dimensions is presented in the following chapter.

III. Monte Carlo Simulation of Heterogeneous Scintillation Detectors

Dr. Harvey H. Ross (Oak Ridge National Laboratory) graciously provided a copy of a Monte Carlo code called Alpha Detector (Copyright 1988) for use in this study. He and L. L. Rozevink designed the code to investigate the geometric efficiency of close packed spherical scintillators; their results and an overview of Alpha Detector have been previously published (Ross, 200-203: 1991). The code was an excellent starting point for the present work, however several modifications to the program were made to allow more flexible modeling and to provide data to produce modeled energy spectra. The revised code is written in QBasic and is referred to as Alpha.bas (included in Appendix A). This chapter presents an overview and results of the modeling accomplished with Alpha.bas.

Model Overview

Geometry. The code models a heterogeneous detector as a structure of spheres arranged in a face centered cubic (FCC) array. The unit cell for such a structure is shown in Figure 3-1. The spheres in a close packed FCC structure occupy essentially 74% of the volume, with a resultant porosity of 26%. In order to model detectors with a variety of porosities, the program calculates the side of the unit cell according to:

$$a = 2r\left[\frac{2\pi}{3(1-n)}\right]^{1/3} \qquad (3\text{-}1)$$

where r is the radius of the spheres
n is the porosity

As an example, Figure 3-2 depicts the modeled unit cell of a 50% porous detector.

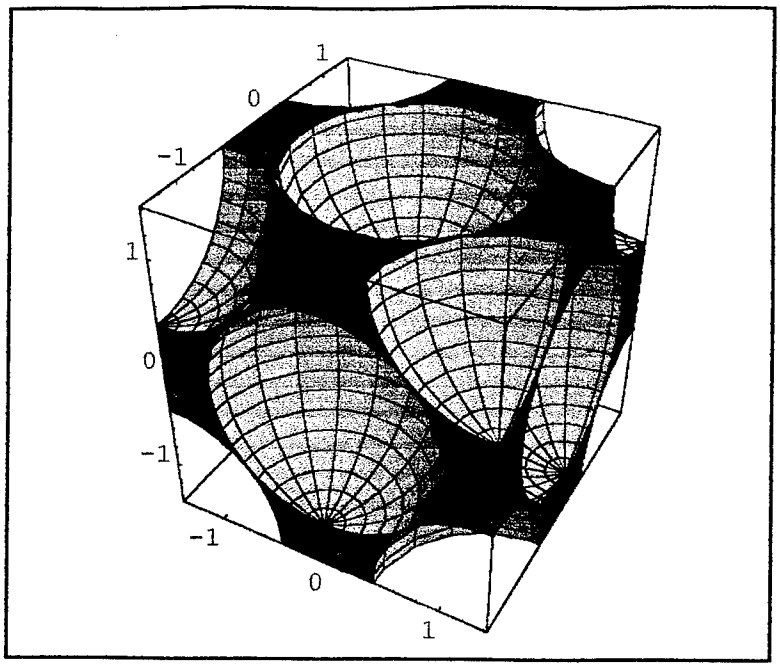

Figure 3-1. Close packed FCC unit cell. This figure depicts the unit cell used by Alpha.bas to model a 26% porous detector.

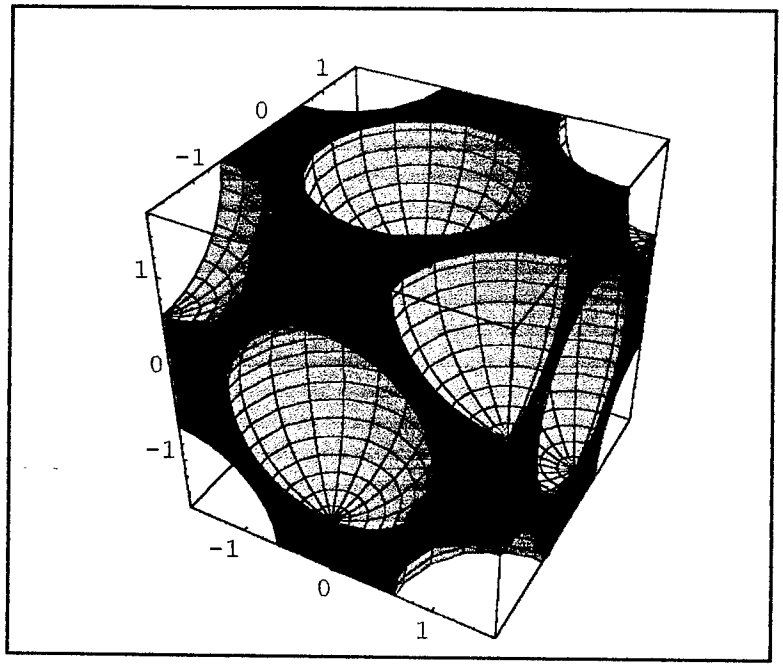

Figure 3-2. 50 % porous FCC unit cell. This is an example of the reduced volume fraction of spheres used to model a higher porosity material. Alpha.bas would use this structure to model a 50% porous material.

Decay Events. The code generates random locations for decay events. One of two modes can be selected by the user: the alpha-emitting nuclides may be generated uniformly distributed through the volume of the pore space[1] (simulating a solution containing the radioisotope within the pores), or uniformly distributed on the surface of the spheres (simulating adsorbed emitters). For each simulated decay event, the program also generates a random direction of travel. Each alpha particle is assumed to move in a straight line from its decay point to the end of its track.

Range and Energy Calculations. Alpha.bas calculates the length of an alpha's track through each sphere and each pore it encounters. The code then calculates the energy remaining to the alpha as it exits the sphere (or pore) by a residual range method (see, for example, Knoll, 41: 1989). The code sums the total energy deposited in spheres along the alpha track, and provides this data as output.

The program finds range values needed for the residual range method by calculating the range of the alpha in air using an empirical fit to experimental data, given by (Ross: 1994):

$$R_a = 0.377E_\alpha^{1.39} \qquad (3\text{-}2)$$

where R_a is the alpha range in air (cm)
E_α is the alpha energy (MeV)

---

[1] I will generally refer to the interstitial space between spheres as the "pores", however the program can also simulate a detector with spherical pores and surface distributed emitters. It does not currently simulate emitters distributed through the volume of spherical pores.

A comparison of this method and experimental data is provided in Figure 3-3. The code relates the range in the user specified material to the range in air according to (Friedlander, et al, 95: 1964):

$$R = \{R_a[C + (0.06 - 0.0043A_e)\log(\frac{E_\alpha}{4})] - 0.0025A_e\}/\rho \qquad (3\text{-}3)$$

where

	R	is the alpha range in the material (cm)
	A_e	is the effective atomic mass of the material
	$C = 1$	for $A_e \leq 20$
	$C = 0.9 + 0.01375A_e$	for $A_e > 20$
	ρ	is the density of the material (mg/cm^3)

The effective atomic mass of a material is calculated according to:

$$A_e = \frac{[dD + eE + fF + \ldots]^2}{\left[d(D)^{0.5} + e(E)^{0.5} + f(F)^{0.5} + \ldots\right]^2}$$

where Capital letters are atomic masses of constituent elements of the material
Lower case letters are atom fractions of each element in the material

User Input. Alpha.bas requires the user to provide the alpha particle energy, sphere radius, porosity (volume fraction of the interstitials), number of events, and the density and effective atomic mass for both materials in the heterogeneous system as input parameters. The program will increment through a series of radius values if requested by the user. The physical parameters used for all materials modeled in this paper are listed in Table 3-1.

Code Output. Alpha.bas stores user input data and detector efficiency results as output. It also stores the energy deposited in spheres for each decay event.

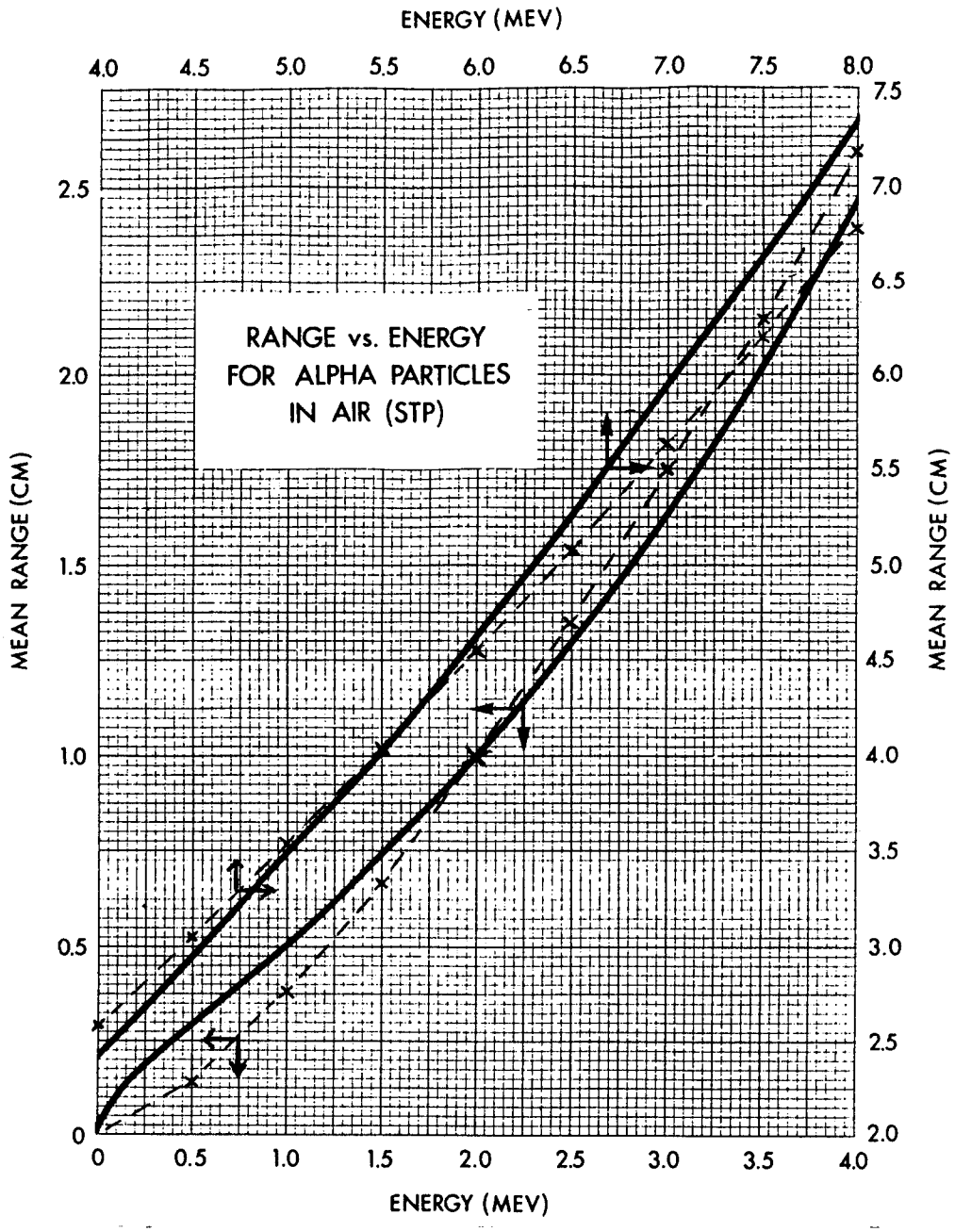

Figure 3-3. Alpha Range in Air. A comparison of the alpha range in air used by Alpha.bas to published experimental data (Knoll, 36: 1989).

Table 3-1. Material Properties Used as Input Parameters

Material	Density (gm/cm^3)	Effective Atomic Mass (gm/mole)
Water	1	13.8
Ultima Gold	0.96	8.18
Polystyrene	1.03	8.24
Gel-silica	2.2	20.38
Glass Beads	2.2	20.38

Post Processing of Data. Frequency distributions of the energy deposited in the active material of the detector are easily generated using spreadsheet or mathematics software packages. Modeled energy spectra in this paper were produced in a MathCad 5.0 Plus worksheet which reads the energy data output from Alpha.bas, generates a histogram of the energy deposited in the scintillator, then imposes a Gaussian system resolution upon that histogram to produce an energy spectrum. The model does not attempt to incorporate the effects of light collection efficiency into the energy spectra produced.

Model Results

Geometric Efficiency. Ross published curves of geometric efficiency vs. polystyrene bead radius produced using his program Alpha Detector (Ross, 206: 1991).

Figure 3-4 is a copy of his results for ^{241}Am in an aqueous solution filling the interstitial space between packed scintillating beads. Alpha.bas yields a similar curve for this heterogeneous system with a volume distributed ^{241}Am source, as seen in Figure 3-5. Results from Alpha.bas indicate attainment of 100% geometric efficiency at a larger sphere radius than found by Ross, as well as a more rapid decrease in efficiency with increasing scintillator radius. These differences occur because Ross's assumption of 74% detection efficiency for alphas which penetrate beyond the first layer of spheres was abandoned. The results from the program Alpha Detector and from Alpha.bas are in qualitative agreement.

Additional information shown in Figure 3-5 includes the results for the case of ^{241}Am adsorbed onto the surface of the scintillating spheres, and two experimental data points published by Ross. Comparison of the two curves in this figure indicates that an adsorbed source yields a significantly higher geometric efficiency than does a source distributed throughout the pore for large radii spheres. These results are consistent with what one would expect in the limit of very large radii spheres (with increasing radius, the geometric efficiency should approach 50% for an adsorbed source, and 0% for a volume distributed source). Ross's experimental data for 68 micron beads is inconsistent with an ^{241}Am source distributed through the inactive phase of his detector, since the measured detection efficiency can never be greater than the geometric efficiency. This data point suggests that the ^{241}Am was partially adsorbed on the scintillating spheres, causing the

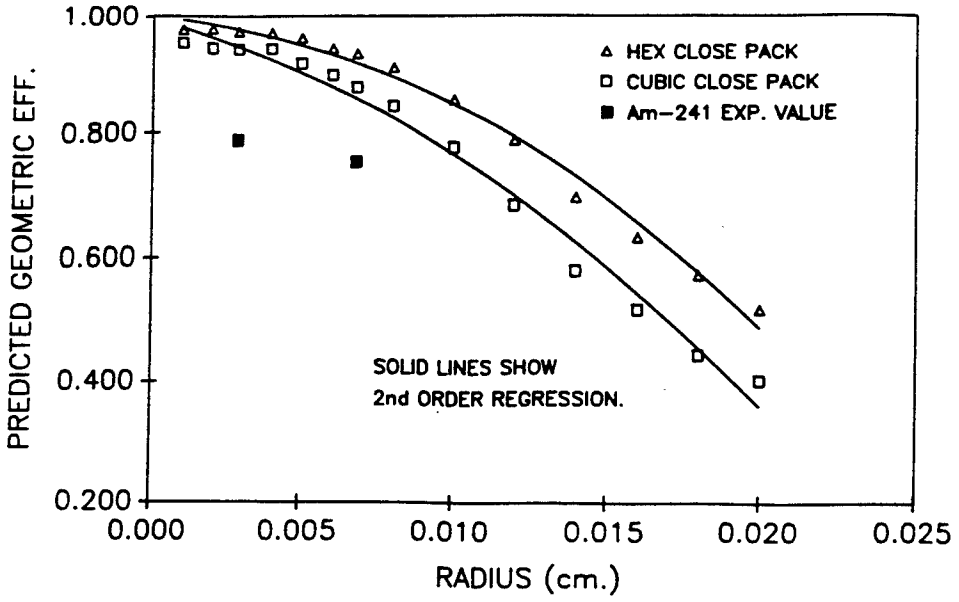

Figure 3-4. Geometric Efficiency vs. Radius. Monte Carlo simulation of Am241 alphas based on the code Alpha Detector, and experimental data (Ross, 206: 1991).

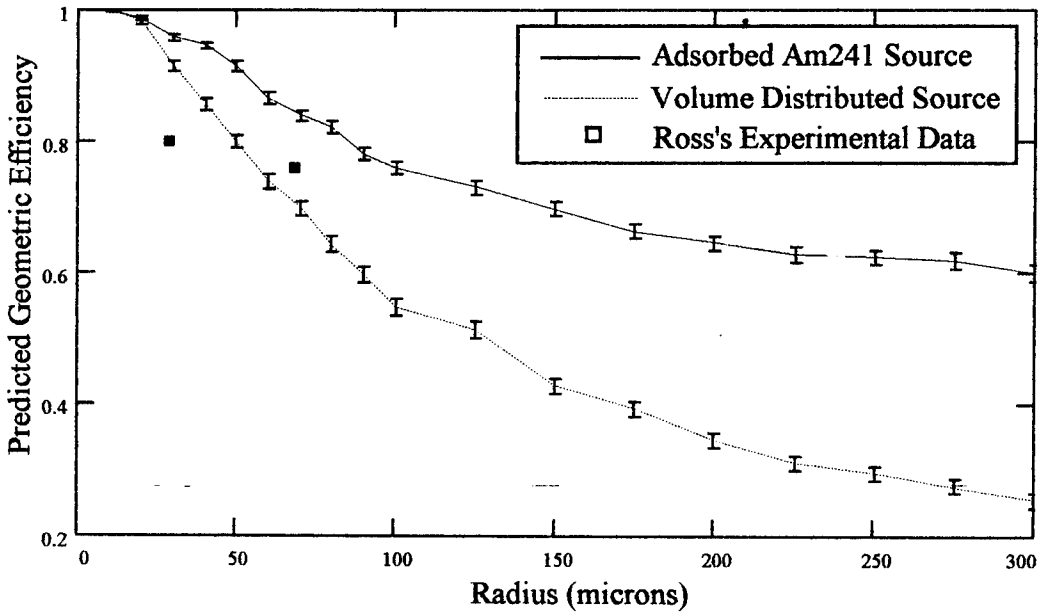

Figure 3-5. Modeled Geometric Efficiency. Each data point is based on a 2000 event run of Alpha.bas. The "I" bars represent the error in the calculated data point, with the data points vertically centered on each "I" bar (errors calculated according to Bevington, 76: 1992). The representation of Ross's experimental data in this figure are based on values read from his published graph (see Fig. 3-4).

measured detection efficiency to fall between the two curves of Figure 3-5. Energy spectra modeled for Ross's detector support this conclusion, as shown in Figure 3-6. The solid line represents a spectrum modeled for a 50% adsorbed source, while the dashed curve is modeled for a source distributed through the pore volume. The full energy peak (FEP) present in the partially adsorbed case is much more consistent with the peak seen in Ross's published experimental data than is the poorly resolved spectrum of the volume distributed source. The reader is referred to Ross's article for his energy spectra, which could not be reproduced here (Ross, 205: 1991).

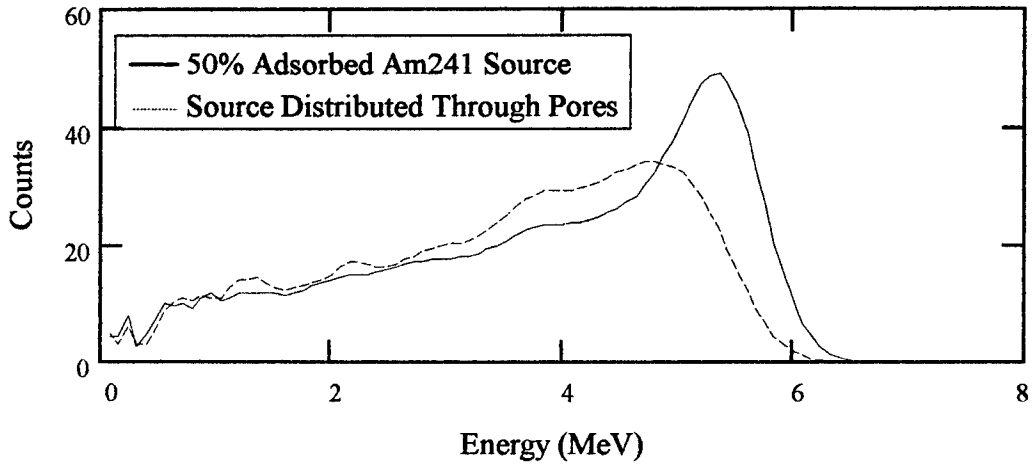

Figure 3-6. Modeled Energy Spectra for Alphas Detected with Polystyrene Spheres. Modeled for Am241 alphas being detected in a cell composed of 70 μm scintillating polystyrene spheres. These spectra are based on Alpha.bas runs of 2000 events each, with a 15% FWHM system energy resolution imposed.

Simulations of a gel-silica matrix with liquid filling the pores indicate that alpha particles emitted within the pore structure should be detected with 100% geometric efficiency, independent of whether the glass matrix or the liquid is the scintillator. This is

not an unexpected result, since alpha particles with MeV energies will transit hundreds of pores in gel-silica with typical pore dimensions on the order of nanometers or less.

Energy Deposition. An alpha particle traversing a large number of pores within a gel-silica monolith will deposit a fraction of its energy in the glass and the remaining energy in the material filling the pores. The fraction deposited in each material can be estimated as follows: start by assuming the shape of the linear energy transfer curve is independent of the stopping medium (Cesini *et al*, 579: 1975):

$$\left[\left(\frac{dE}{dx}\right)_0\right] = k\left[\left(\frac{dE}{dx}\right)_1\right] \qquad (3\text{-}4)$$

where

$(dE/dx)_0$	is the linear energy transfer into material 0
$(dE/dx)_1$	is the linear energy transfer into material 1
k	is a proportionality constant to be determined
x	is a dimensionless length which has been scaled by the range of the alpha in each material

We can write the range in each material as:

$$R_0 = \int_{E_\alpha}^{0} \left[\left(\frac{dE}{dx}\right)_0\right]^{-1} dE \qquad (3-5)$$

and

$$R_1 = \int_{E_\alpha}^{0} \left[\left(\frac{dE}{dx}\right)_1\right]^{-1} dE = k\cdot\int_{E_\alpha}^{0} \left[\left(\frac{dE}{dx}\right)_0\right]^{-1} dE \qquad (3-6)$$

Combining Equations 3-4, 3-5, and 3-6 yields:

$$\frac{R_1}{R_0} = \frac{k\int_{E_\alpha}^{0}\left[\left(\frac{dE}{dx}\right)_0\right]^{-1}dE}{\int_{E_\alpha}^{0}\left[\left(\frac{dE}{dx}\right)_0\right]^{-1}dE} = k \qquad (3-7)$$

We now use the Bragg-Kleeman rule to relate the particle ranges in the two materials (see, for example, Knoll, 43: 1989), and assume that the atomic mass can be replaced with an effective atomic mass for each compound:

$$k = \frac{R_1}{R_0} \cong \frac{\rho_0'}{\rho_1'}\sqrt{\frac{A_{e_1}}{A_{e_0}}} \qquad (3\text{-}8)$$

The primes indicate densities which are reduced from the bulk material densities by the volume fraction of each material. Replacing the primed densities with bulk densities leads to:

$$k \cong \frac{n}{1-n}\left[\frac{\rho_0}{\rho_1}\right]\sqrt{\frac{A_{e_1}}{A_{e_0}}} \qquad (3\text{-}9)$$

Where n is the volume fraction of material 0. Substituting this value for the proportionality constant into Equation 3-4 and integrating over the range of an alpha in each material yields:

$$\frac{E_0}{E_1} \cong \frac{n}{1-n}\left[\frac{\rho_0}{\rho_1}\right]\sqrt{\frac{A_{e_1}}{A_{e_0}}} \qquad (3\text{-}10)$$

where E_0 is the total energy deposited in material 0

E_1 is the total energy deposited in material 1

We know that $E_0 + E_1 = E_\alpha$, so

$$E_0 \cong E_\alpha \left[\frac{1-n}{n} \left(\frac{\rho_1}{\rho_0} \right) \sqrt{\frac{A_{e_0}}{A_{e_1}}} + 1 \right]^{(-1)} \tag{3-11}$$

and

$$E_1 = E_\alpha - E_0 \tag{3-12}$$

Figure 3-7 is a plot of energy deposited in scintillation cocktail as a function of porosity of a porous glass detector. The upper curve represents the results obtained with Equation 3-11, while the lower curves were produced by using output from Alpha.bas. Points produced with a modification of Alpha.bas using the Bragg-Kleeman relationship, Equation 3-8, in place of Equation 3-3 are marked with x's. Note that results from the modified code are in excellent agreement with Equation 3-11, indicating that the residual range method employed by the program is working properly. The lower values produced by Alpha.bas are a result of the use of Equation 3-3 rather than the Bragg-Kleeman relationship for the range calculations.

The dashed and dotted curves in Figure 3-7 represent markedly different pore geometries. The dashed curve shows a simulation of 0.1 μm spherical pores filled with Ultima Gold (a liquid scintillation cocktail distributed by Packard), while the dotted curve represents the scintillation cocktail in the interstices between 0.1 μm spheres. The results indicate that the fractional energy deposition in the two materials has a slight dependence on pore geometry. The square and "+" markers in Figure 3-7 are values for single-event

runs of Alpha.bas which simulate Ultima Gold filling the 3 nm pores (see legend). These markers fall atop the curves for much larger radii spheres, indicating that the fractional energy deposited in each material is independent of the pore dimension (at sub-micron dimensions). Thus for a given gel-silica detector composition, the fractional energy deposition is essentially a function of porosity only.

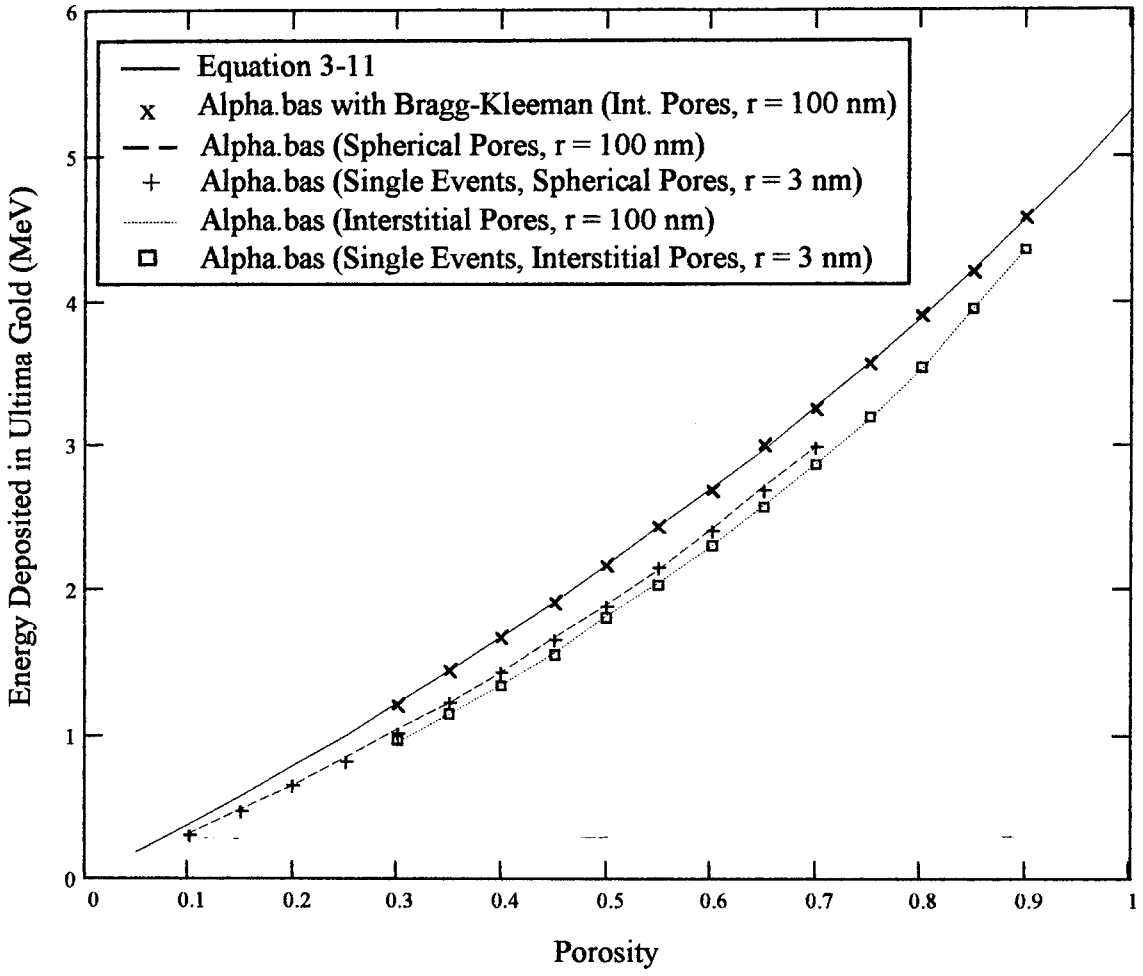

Figure 3-7. Energy Deposited in Ultima Gold vs. Porosity. This is a comparison of theoretical and modeled energy deposition in liquid scintillator filling a porous glass cell. Points marked with x's were generated using a version of Alpha.bas modified to use the Bragg-Kleeman relationship in place of Equation 3-3. All other modeling results presented in this paper used Equation 3-3.

Intrinsic Energy Resolution. The idea of an intrinsic energy resolution associated with a heterogeneous scintillation detector was introduced in Chapter 2. Essentially, the amount of energy each alpha particle deposits in the active phase will depend upon its path through the detector. Variations in this deposited energy will result in a statistical broadening of the energy line width based solely on the two phase nature of the detector. Intrinsic energy resolutions presented here are calculated as the full width at half maximum (FWHM) divided by the mean value of Gaussian fits to modeled energy distributions. This section presents the results of modeling the intrinsic energy resolution capability of monolithic gel-silica detectors and particulate detectors.

For gel-silica materials with pore dimensions less than 10 nm, simulations indicate the amount of energy deposited in each material is well-defined. Results show intrinsic resolutions on the order of 0.5 % or better for energy deposited in the glass phase of a 40% porous detector. The intrinsic energy resolution shows a linear dependence on pore radius, as seen in Figure 3-8. This is not a surprising result, as the spread of energies which could be deposited in a pore would be determined by the pore dimension. The modeled data in Figure 3-8 show that 40% porous detectors with pore radii below 10 nm would have intrinsic energy resolutions better than 0.5% for energy deposited in the glass. In this example, the resolution to be expected for the liquid phase is poorer than for the glass phase because the spread in energies deposited is the same for each phase, yet less energy goes into the liquid than into the glass.

The intrinsic resolution of an actual liquid-filled gel-silica is likely to be slightly poorer than the modeled values due to the distribution of pore geometries and sizes

contained in gel-silica, as well as the random nature of the structure (as opposed to the regular array modeled). However, the dependence of energy deposition on pore size and geometry is not strong (see Figure 3-7), and narrow pore size distributions are available in gel-silica (Hench, et al, Figure 3: 1993). Thus, the model should have reasonable accuracy in predicting the intrinsic resolution capability of an actual gel-silica sample.

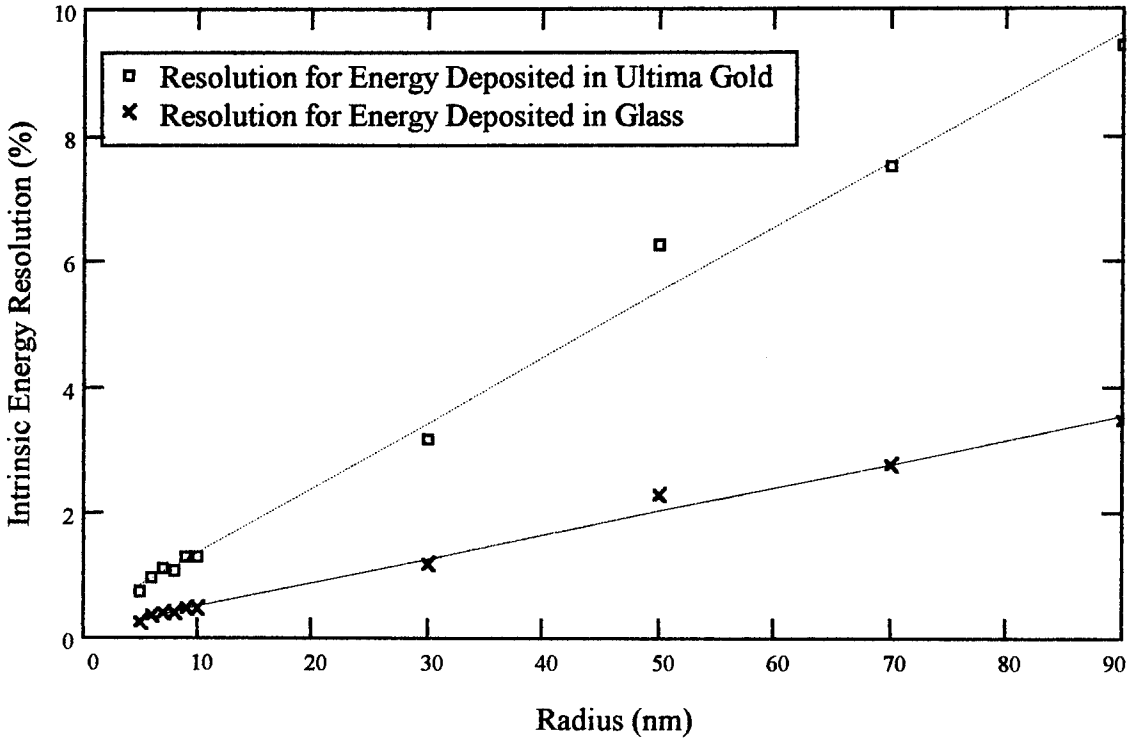

Figure 3-8. Intrinsic Energy Resolution vs. Radius. Modeled results for both phases of a 40% porous detector are shown, with least squares linear fits. The data points for both cases are based on one set of data. FWHM resolutions are based on Gaussian fits to 100 event runs of Alpha.bas for the points below 10 nm, and 500 event runs for the points at 10 nm and above.

The intrinsic resolution available from liquid-filled gel-silica will not be the limiting factor on system resolution for a system utilizing such a detector. Improvements in

photon generation and light collection will be required before the intrinsic energy resolution capability of a heterogeneous gel-silica system could be reached. This is not necessarily true of particulate detectors, where choosing the wrong particle size may destroy any chance of performing spectroscopy with the detector.

Figure 3-9 depicts a series of histograms showing the modeled energy deposited in spheres for four different radii of polystyrene spheres with an adsorbed ^{241}Am source and water filling the pores. These figures show the transition from a well resolved fractional energy deposition at sub-micron radii, through a region of poor intrinsic energy resolution at intermediate radii, to an essentially monoenergetic FEP at large radii. The results of imposing a 10% FWHM Gaussian system resolution upon the histograms in Figure 3-9 are depicted in Figure 3-10. In this example, the energy resolution of the detection system would be limited by the intrinsic energy resolution capability of the detector for the 1 micron and 10 micron scintillating spheres. The resolution would be limited by the 10% system capability in the case of small and large particle radii.

Figure 3-11 depicts the same modeled detectors, with the ^{241}Am distributed through the pore volume. Comparison of Figures 3-9 and 3-11 shows that the intrinsic resolution available at small pore dimensions becomes independent of the source distribution. The volume-distributed source results in a more rapid transition to poor resolution as the sphere radius is increased. An FEP does not emerge as the radius is further increased in the case of a source distributed through the non-scintillating media.

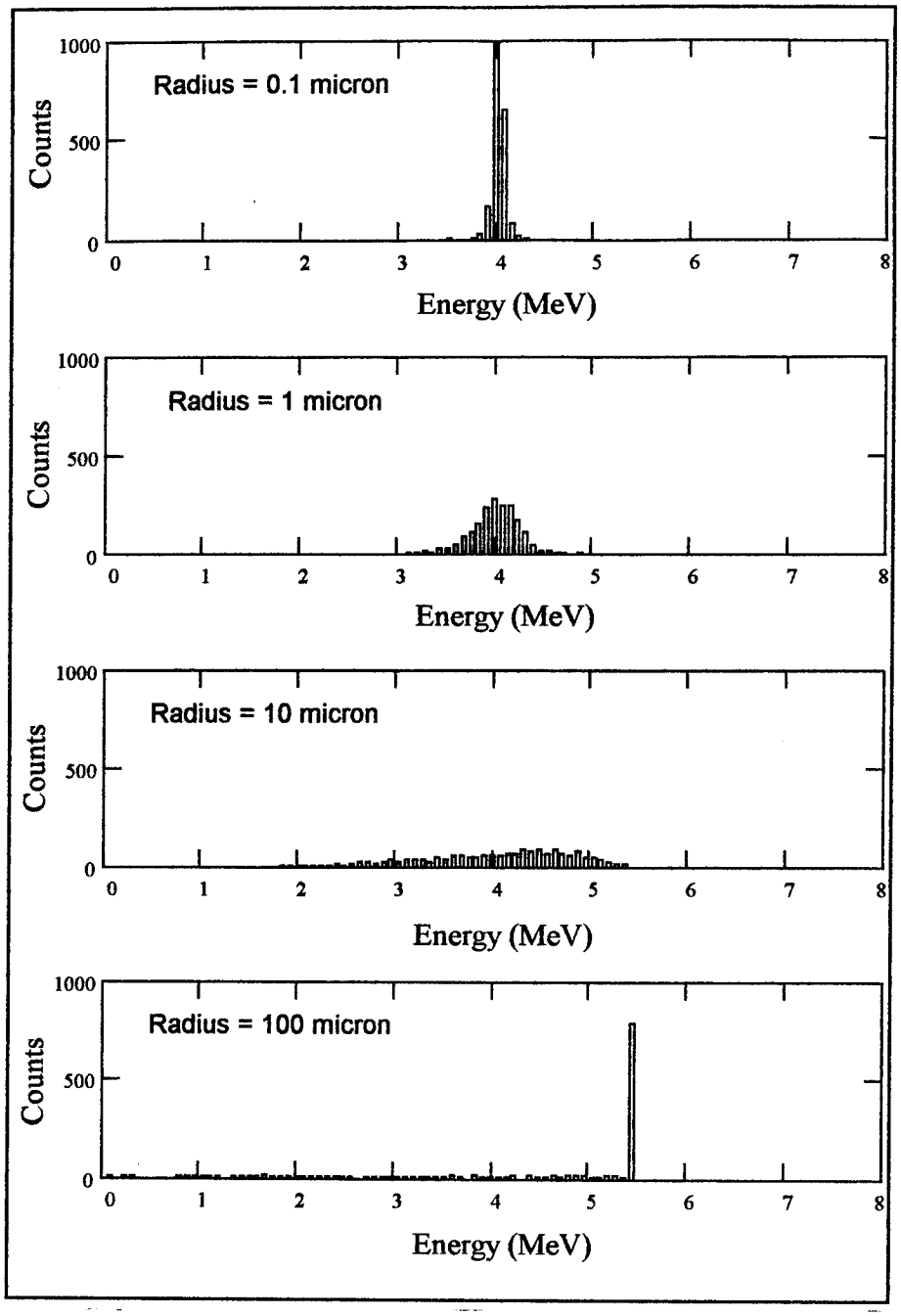

Figure 3.9. Modeled alpha energy deposition in polystyrene spheres from an Am241 source adsorbed on the sphere surfaces. This sequence shows the transition from good intrinsic energy resolution at small particle sizes to poor resolution with increasing phase dimensions. The emergence of a sharp energy peak associated with essentially 50% of the alphas depositing their full energy in large radii spheres is seen in the lowest frame.

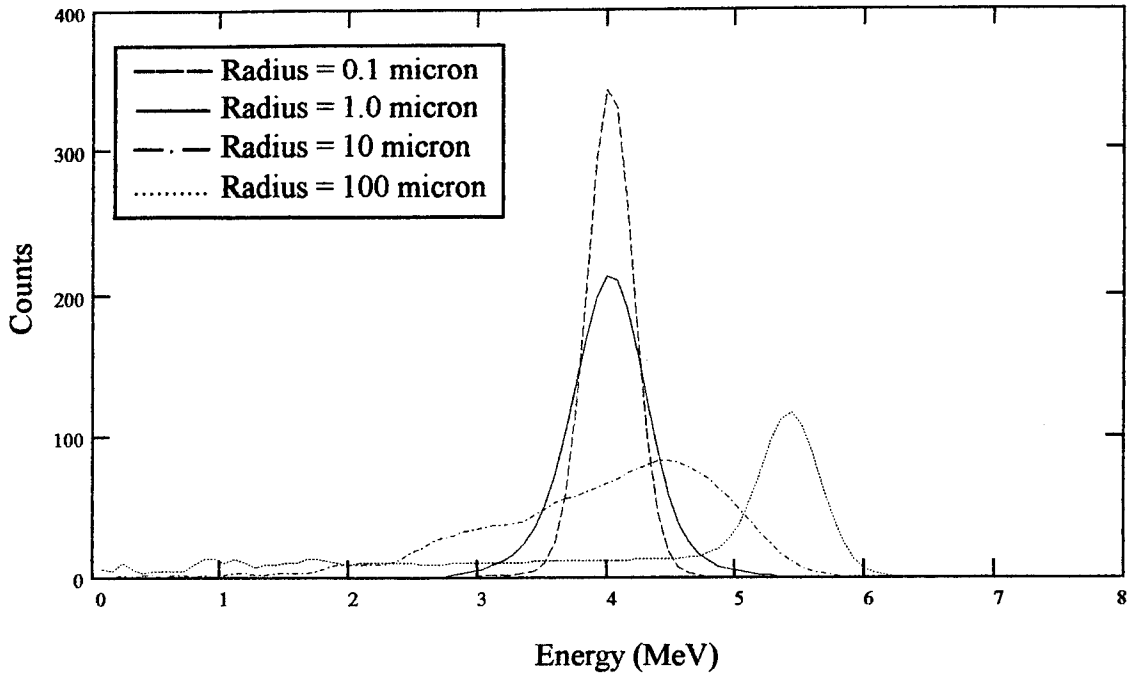

Figure 3-10. Modeled Energy Spectra. Based on systems using scintillating polystyrene beads of four different radii with a 10% system energy resolution capability.

Simulations with Alpha.bas indicate that heterogeneous scintillation detectors can provide very good intrinsic energy resolution at small pore sizes. A transition region exists at intermediate particle sizes where the intrinsic resolution is poor. A detector constructed of large spheres can provide good intrinsic resolution for an adsorbed source, however the resolution will be very poor for a source distributed within the non-scintillating medium. It should be noted that the definitions of small, intermediate, and large particle sizes depends on the energy of the alpha particles of interest. Practically, this means that the poorest intrinsic energy resolution at small particle sizes will occur for the lowest energy alphas being detected. Conversely, large spheres are large relative to the range of the highest energy alpha particles in the spheres.

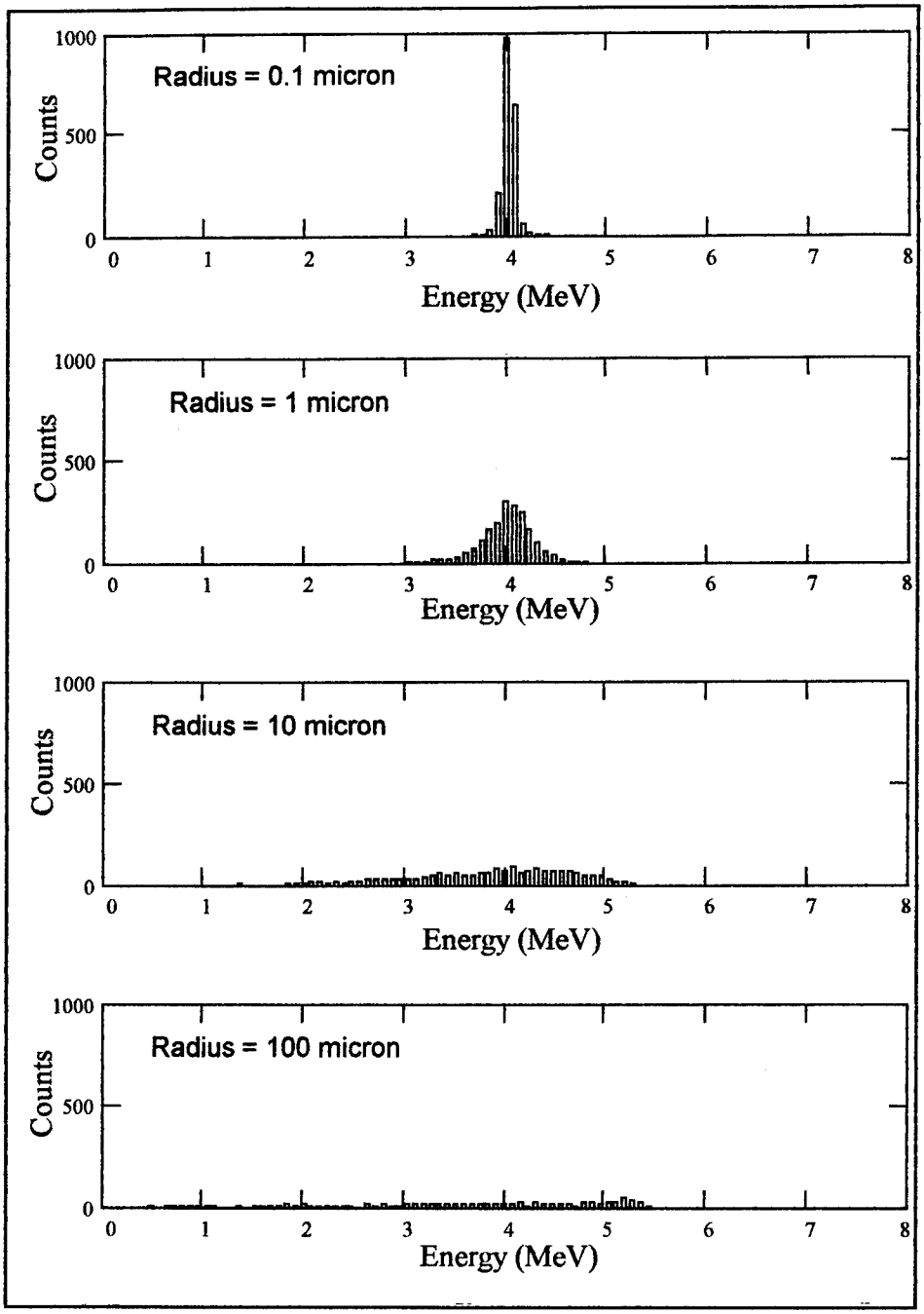

Figure 3.11. Alpha energy deposition in polystyrene spheres from an Am241 source distributed through the pore volume. At small radii, the intrinsic energy resolution is similar to that achieved by an adsorbed source (see Figure 3-10). However, the peak associated with alphas depositing their full energy in large radii spheres does not emerge in this case.

Model Predictions Tested Experimentally

The modeling of heterogeneous scintillation detectors discussed in this chapter provides predictions that should be readily verified in the lab. To investigate the low end of the dimensions modeled, experiments intended to determine the fractional energy deposition and alpha detection efficiencies in gel-silica samples were performed. At large dimensions, the dependence of detection efficiency on the distribution of emitters was probed using glass spheres with radii on the order of 75 μm. The model predictions for these cases are presented below.

Fractional Energy Deposition. The energy deposited in Ultima Gold vs. porosity for Ultima Gold in gel-silica was presented in Figure 3-7. Gel-silica with 2 nm pores and 30% porosity were modeled to correspond to the samples used for the experimental portion of this project. For these parameters and 5.304 MeV ^{210}Po alpha particles, Alpha.bas predicts deposition of 1.011(.001) MeV in the liquid phase (based on spherical pores). In the case of alpha particles being emitted from within the pore structure, a single peak is expected in the energy spectrum, as depicted in Figure 3-12.

Although not anticipated prior to the experimental work, spectra indicating polonium deposits on the exterior surface of gel-silica samples were also encountered. The modeled spectra in such a case consists of a peak representing fractional energy deposition in the pores, and an FEP due to alphas leaving the surface and depositing their full energy in bulk scintillation cocktail. In the case of an ideal surface layer of polonium, these peaks have equal areas, since 50% of the alphas move into the sample, and 50%

move away from the sample in the case of isotropic decay. The modeled energy spectra for such a surface layer of polonium, detected in a system with 20% FWHM energy resolution, is shown in Figure 3-13.

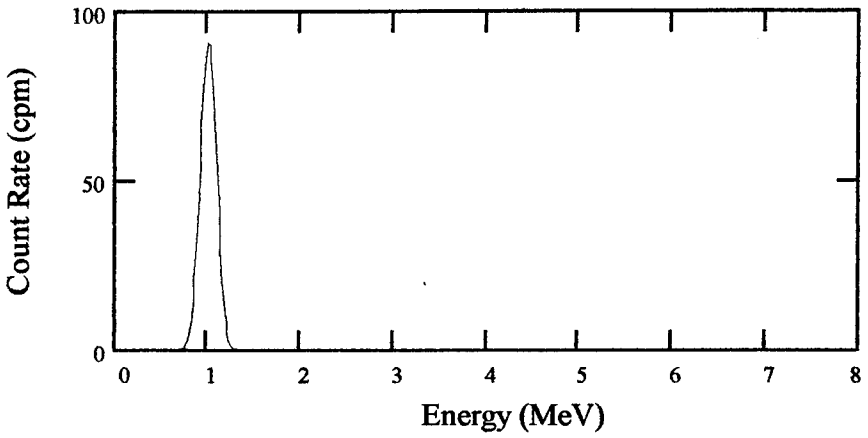

Figure 3-12. Modeled Energy Spectrum for Polonium in Gel-silica. Based on 5.304 MeV Po210 alphas deposited in the pores of liquid scintillant filled gel-silica, with a detection rate of 1000 cpm and a system resolution of 20%.

Detection Efficiency in Gel-silica. Alpha particles should be detected with 100% geometric efficiency if they originate from within the nanometer-scale pore structure of a liquid scintillation filled gel-silica sample.

Detection Efficiency in Glass Bead and Liquid Scintillator Matrix. Figure 3-5 indicated that heterogeneous detectors constructed of large size spheres will have significantly different geometric efficiencies depending on whether the emitters are adsorbed on the sphere or distributed through the volume of the pores. Similar differences occur in the case of liquid scintillator filling the pores between inert beads, however the

geometric efficiency is higher for the volume distributed source in this case. This difference was investigated for a glass bead (75 μm mean radius) and liquid scintillator matrix which was roughly 33% liquid scintillator by volume. Model results indicate that such a matrix has a 100% geometric efficiency for detecting alphas emitted by a source distributed within the liquid phase. On the other hand, alphas emitted at the surfaces of the spheres should be detected with a 57.2% geometric efficiency. Figure 3-14 shows the modeled energy spectra for these two cases, however it is expected that the poor light collection properties anticipated for such a cell would significantly degrade these spectra.

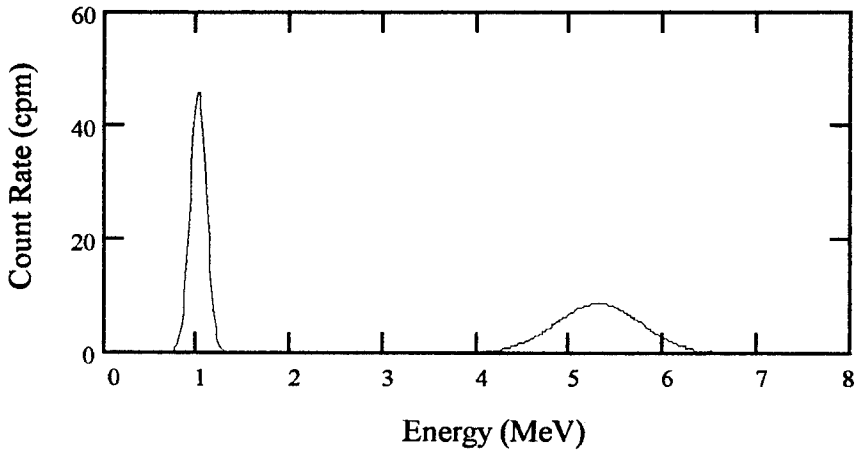

Figure 3-13. Energy spectrum modeled for a surface deposit of Po210 on gel-silica. Based on a count rate of 1000 cpm and a system resolution of 20%.

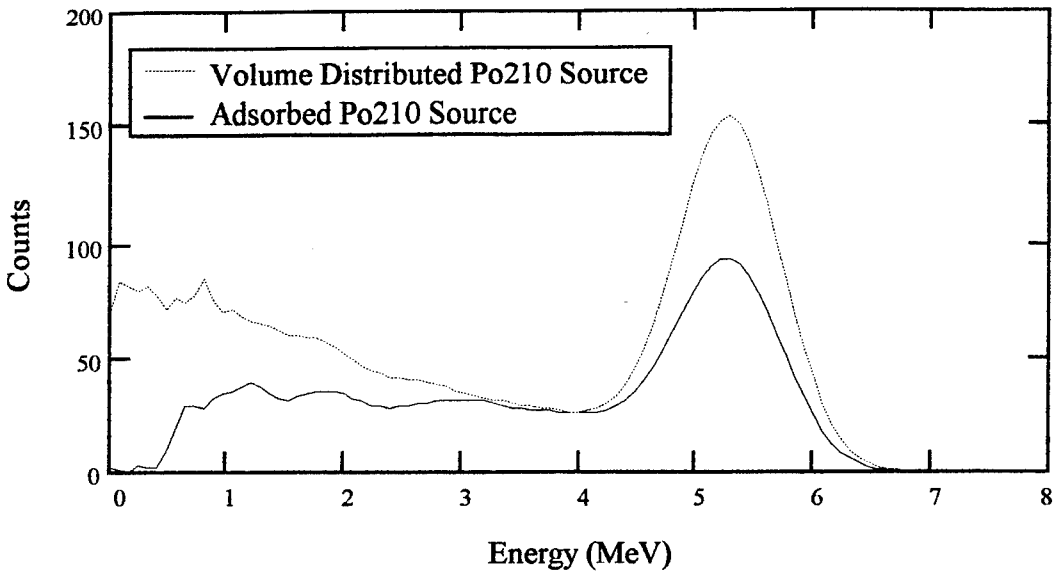

Figure 3-14. Energy spectra modeled for detection of Po210 alphas in a detection cell constructed of glass beads with 75 μm radii. Based on 5000 event runs of Alpha.bas for each trace, with the assumption of 33% porosity and a system resolution of 20%.

IV. Experimental

Introduction

The experimental portion of this project initially focused on investigating the scintillation properties of cerium doped gel-silica. Unfortunately, the first samples received from the University of Florida displayed no scintillation pulses. Because of the long lead time involved in processing gel-silica samples, the focus was shifted to heterogeneous systems where the scintillation occurred in the liquid phase of the detector.

Variations on two experiments were performed to investigate alpha energy deposition in heterogeneous detectors. In one experiment, energy spectra were obtained from gel-silica samples doped with ^{210}Po and immersed in liquid scintillation cocktail. One objective was to verify the fractional energy deposition in scintillant within the pores of the gel-silica. Another goal was to determine the efficiency for detecting alphas emitted within the sample. Insight into the effects of the two-phase structure on energy resolution was also desired. The second experiment consisted of counting alphas in a glass bead and liquid scintillator cell. The intent was to experimentally verify the modeled difference in counting efficiencies for adsorbed and volume distributed alpha emitters at large particle sizes.

This chapter consists of a discussion of the equipment and materials used to perform these experiments, followed by coverage of general experimental procedures. Procedures peculiar to a particular experiment are presented immediately prior to the

results for that experiment. Results are presented in the sequence of the objectives discussed above, along with comparison to the model predictions presented in the last chapter.

Equipment and Materials

Liquid Scintillation System. A Packard Tri-Carb 2200CA Liquid Scintillation Analyzer (Serial Number 101559) was used to obtain all energy spectra and counting data which follow. The system uses two photomultiplier tubes (PMTs) operated in coincidence mode to reduce background counts caused by spurious pulses in the PMTs. Coincident pulses from the PMTs are summed and sorted by pulse height into an integrated 4000 channel multichannel analyzer (MCA) to form energy spectra. The bin size for spectra in this paper has been doubled by summing counts in adjacent bins to make them coincide with the visual and hard copy spectra provided by the system.

Additional Equipment.

Scale: Mettler AT 261 DeltaRange Balance

Micropipettes: Excaliber 1 - 5 and 5 - 50 μl micropipettes by Ulster

Vials: 2 ml translucent vials distributed by Packard

Gel-silica. Gel-silica samples were provided by Dr. Jon West, University of Florida. All samples doped with polonium originated from a single disk (0.5 cm thick, 2 cm diameter) which had cracked into shards early in the investigation. The shards were irregularly shaped, with masses on the order of 0.1 gram. They were transparent with a slight haze when dry, and appeared very clear when the pores were filled with liquid. The

physical properties of samples of gel-silica from the same batch have been published (Hench, *et al*: 1993). The properties most pertinent here are the 30% porosity and an average pore radius of 2 nm.

Glass Beads. Applied Science Laboratories 80/120 mesh silicone glass beads were used. This mesh size corresponds to bead radii ranging from 62.5 μm to 88.5 μm.

Scintillation Cocktail. Packard Ultima Gold scintillation cocktail was used for the liquid scintillation counts reported here. Ultima Gold is a "blend of alkylnaphthalene with scintillators PPO and bis-MSB and emulsifiers." (Packard, 1: 1990) The chemical names for these two fluors are 2,5-diphenyloxazole (PPO) and p-bis(o-methylstyryl) benzene (bis-MSB). The secondary scintillant in Ultima Gold, bis-MSB, results in a fluorescence spectrum peaked at 425 nm.

Polonium Solutions. Dr. George John recommended the use of ^{210}Po for this project based on two desirable properties. First, ^{210}Po emits 5.304 MeV alphas with no other radiations above a yield of 0.001% (Sowby, 1034: 1983). Second, it was available through a straight-forward extraction from an RaDEF solution which was available in the laboratory. RaDEF is the term for a mixture of ^{210}Pb and its daughters, which follow the decay chain:

$$^{210}\mathrm{Pb} \xrightarrow[22.3\ \mathrm{yr}]{\beta^-} {}^{210}\mathrm{Bi} \xrightarrow[5.01\ \mathrm{day}]{\beta^-} {}^{210}\mathrm{Po} \xrightarrow[138.4\ \mathrm{day}]{\alpha} {}^{206}\mathrm{Pb}$$

^{210}Po was extracted from the RaDEF solution by deposition of the polonium onto a silver needle. Three solutions containing ^{210}Po were made by removing polonium from the silver. The first was formed by pipetting NaOH solution over the silver needle, while the second was made by dripping reagent grade hydrochloric acid over the needle. Reagent grade nitric acid was used to remove polonium from the silver for the third solution (see Appendix B). The first two solutions were assigned local identification numbers 247b and 247c, respectively. The third was made up in the same container as #247c, and is designated 247c'.

Knowledge of the specific activity of all three solutions was required to enable calculation of detection efficiencies for samples doped with these solutions. The polonium activity was quantified by liquid scintillation counting of 10 μl samples of each solution, with the assumption of 100% alpha counting efficiency. Tables 4-1 through 4-3 contain the results of these measurements.

Table 4-1. Activity Measurements of Source Solution #247b

Vial ID	Solution Added to Vial (mg)	Time (Local)	Length of Count (min)	Activity (dpm(2σ))
Po10	9.85(0.05)	27 Jul/1026	10	5427(47)
		27 Jul/1313	10	5443(47)
Po11	10.92(0.05)	27 Jul/1036	10	3715(38)
		27 Jul/1323	10	3723(38)

Table 4-2. Activity Measurements of Source Solution #247c

Vial ID	Solution Added to Vial (mg)	Time (hr)	Length of Count (min)	Activity (dpm(2σ))
Po12	10.23(0.05)	3.6	100	55.5(1.8)
		48.8	60	56.5(2.2)
		336.5	60	52.9(2.2)
		346	360	50.8(0.9)
		489	360	50.0(0.9)
Po13	10.52(0.05)	5.8	100	56.7(1.8)
		49.8	60	55.1(2.2)
		352	360	51.5(0.9)
		495	360	48.7(0.9)

Times are referenced to an initial time of 1200 EDT on 9 Aug 94.

Table 4-3. Activity Measurements of Source Solution #247c'

Vial ID	Solution Added to Vial (mg)	Time (hr)	Length of Count (min)	Activity (dpm(2σ))
Po20	9.73(0.05)	18.5	15	5561(48)
Po25	9.68(0.05)	107.5	15	5554(48)

Times are referenced to an initial time of 0000 EDT on 7 Sep 94.

Measurements of the activity of solution 247b yielded inconsistent results, indicating a non-uniform distribution of ^{210}Po in the solution. The values in Table 4-1 show a difference in activity of more than 30% between two samples drawn from the solution. A previous attempt to determine the activity yielded similarly disparate results. One possible explanation for these difficulties lies with the sodium hydroxide solution used

in preparing source solution 247b. This solution had been in a glass bottle for a long period, perhaps years, allowing a significant amount of colloidal silica to form in the solution. Coagulation of these silica colloids may have occurred due to heating of the sodium hydroxide solution under a heat lamp (Iler, 555: 1979), or due to the introduction of polonium into the solution. Polonium would adsorb onto these colloids (Figgins, 19: 1961), forming a non-uniform solution with suspended particles containing varying amounts of the radionuclide. This hypothesis is supported by the multiple peaks which were observed in spectra from these samples (see Figure 4-1), where a single FEP from ^{210}Po is expected The peak which is roughly 1 MeV below the FEP in Figure 4-1 may be the result of alphas spending the initial portion of their tracks transiting silica particles on

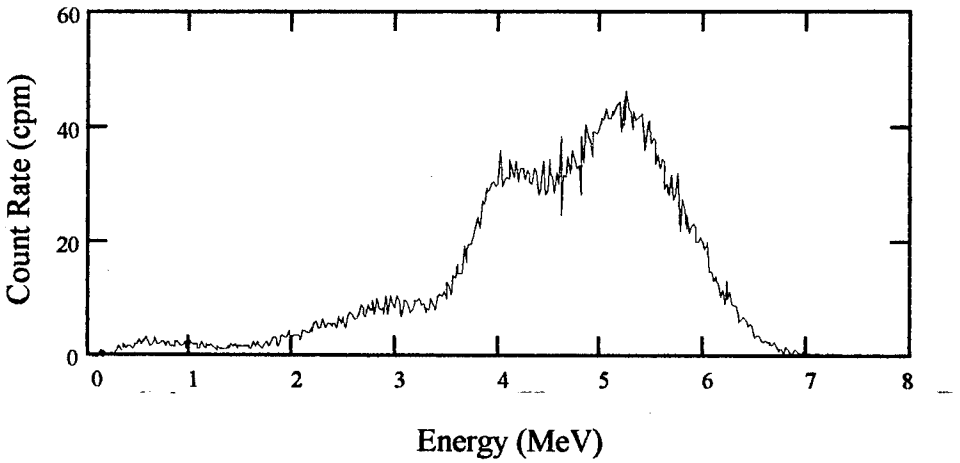

Figure 4-1. Po210 spectrum from a sample of source solution 247b in Ultima Gold. A single FEP is expected at 5.304 MeV. Degradation of counts to lower energy may be due to alpha energy loss within particles formed by coagulation of silica colloids.

the order of 5 microns in diameter. Formation of particles of this size would not be unprecedented (Iler, 563: 1979). Due to these results, it was not possible to determine the activity contained in solution 247b, nor detection efficiencies for samples doped with solution 247b. The problems encountered in characterization of this solution prompted creation of the second source solution, 247c.

The specific activity of solution 247c was determined to be:

$$A(t) = 5.33(0.04)\exp(-\lambda t) \quad \text{(dpm/mg)} \qquad (4\text{-}1)$$

where λ is the decay constant for ^{210}Po
t is time measured from t = 0 at 1200 EDT on 12 Aug 94

Equation 4-1 is based on a fit of the exponential decay curve for ^{210}Po to the data listed in Table 4-2, weighted by the uncertainty in the measurements (Bevington, 59: 1992). Figure 4-2 is a plot of specific activity vs. time, and shows the data points in Table 4-2, along with the fit to the data. This fit was used as the known specific activity of solution 247c for subsequent detection efficiency calculations.

The specific activity of solution 247c' was determined to be:

$$A(t) = 5630(69)\exp(-\lambda t) \quad \text{(dpm/mg)} \qquad (4\text{-}2)$$

where λ is the decay constant for ^{210}Po
t is time measured from t = 0 at 0000L on 07 Sep 94

Equation 4-2 is based on a least squares fit to the data listed in Table 4-3, and was used as the known specific activity of solution 247c' for subsequent detection efficiency calculations.

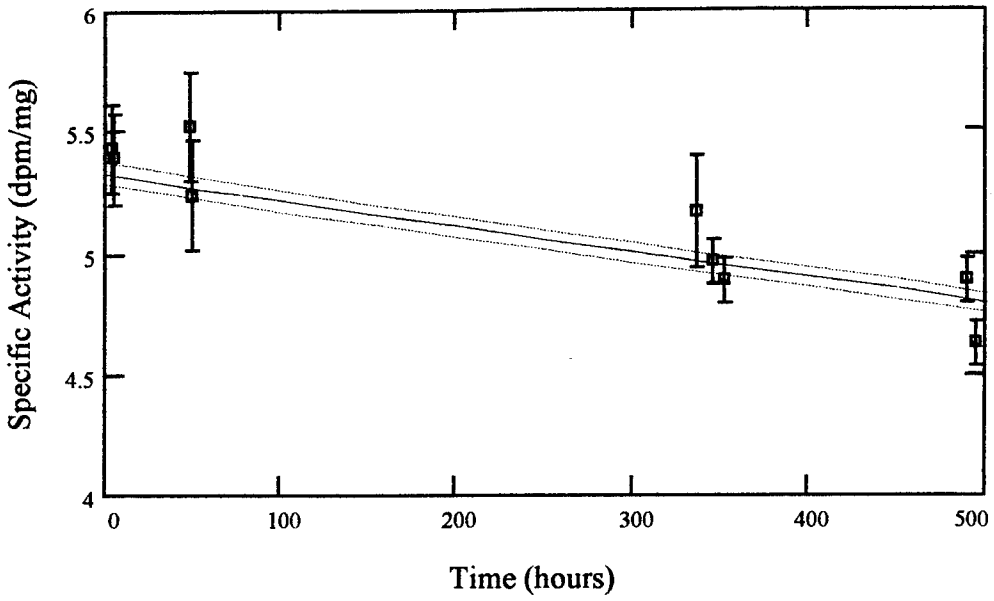

Figure 4-2. Specific activity of polonium source solution 247c.

Procedures

The following general procedures were used to process gel-silica and glass bead samples.

Polonium Doping. Samples were doped with polonium by micropipetting polonium solution onto the sample. The samples were weighed before and after addition of the solution, and both the volume and mass of solution added to the sample were recorded. In the case of gel-silica samples, the solution was micropipetted onto a surface, and could be seen moving into the material. After samples were doped, they were dried under a heat lamp. For experiments using glass beads, the doping and drying were done with the beads in a counting vial. Additional beads were added to the vial to ensure the polonium deposit was not at the top surface of the beads. To investigate the case of

polonium distributed through the pore volume, the scintillation cocktail was doped and counted, then undoped glass beads were added to the vial.

Counting. Samples were typically counted in the liquid scintillation counting system prior to the addition of scintillation cocktail, and again after Ultima Gold was pipetted into the counting vial. Count times varied according to the activity of the sample, and are reported with the results where pertinent. Background counts were taken using sample vials containing materials similar to the count of interest, lacking only the polonium doping. All experimental spectra presented in this paper have had background spectra subtracted.

Addition of Liquid Scintillation Cocktail. Ultima Gold was pipetted into the counting vials. The volume of cocktail used, as well as the surface level of the liquid, varied between samples. One cause for differences was the non-uniform sizes of the samples, which led to different surface levels when the same volume of cocktail was added to samples. For alpha counting, these variations in the volume of cocktail have essentially no effect on the counting efficiency. Differing volumes of scintillant do lead to variations in the light collection efficiency between samples, which means that the energy calibration required varied between samples. For this reason, each spectrum presented in this paper was calibrated individually based on the mean energy of the FEP present in the spectrum or in a related spectrum. Calibration information is provided in the caption for each energy spectrum displayed.

Results and Discussion

Results of the experiments performed for this project are presented in this section, along with discussion of the results and comparisons to the model predictions of Chapter 3. A weak fluorescence observed in both the gel-silica and the glass beads is discussed first, since this phenomenon plays a role in several of the subsequent results to be discussed. The experimental verification of fractional energy deposition within the pores of gel-silica follows. Results pertaining to alpha detection efficiencies and energy resolution in gel-silica are covered in turn. Finally, detection efficiencies in a glass bead and liquid scintillator matrix are presented.

Fluorescence in Silica Glass. Many of the samples prepared were counted after being doped with polonium and dried, but prior to the addition of liquid scintillator. These counts revealed scintillation occurring in the glass itself, which has been previously reported by other researchers (Birks, 579: 1964). The light output and detection efficiencies for these scintillations were very low. The energy spectrum shown in Figure 4-3 is an example of the scintillation seen in polonium doped glass beads. This spectrum displays a peak at very low energy and represents a counting efficiency of 3.7(0.2)%. Peaks which are the result of this fluorescence appear in several of the energy spectra which follow, and will be discussed in relation to those spectra.

Fractional Energy Deposition. All spectra taken using polonium-doped gel-silica samples immersed in Ultima Gold displayed a peak at energies which corresponded well with the expected energy deposition of 1 MeV. The spectra contained other interesting features as well, which are described in following paragraphs. The two samples doped

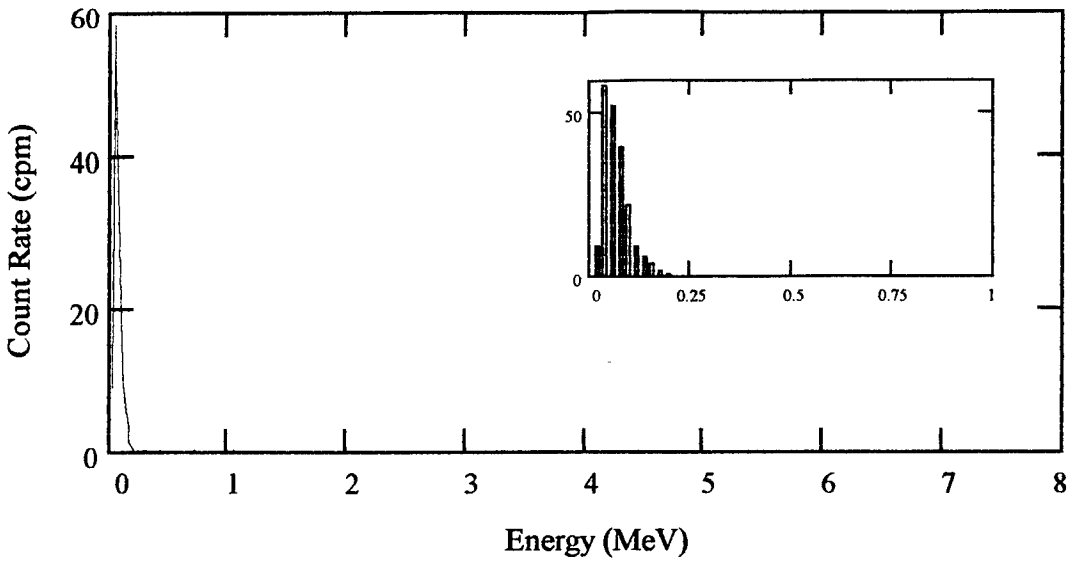

Figure 4-3. Peak observed for Po210 on glass beads with no scintillation cocktail present. An expanded view of the energy histogram from 0 to 1 MeV is inset. This peak represents a detection efficiency of 3.7%.

with solution 247b yielded spectra which correspond well with that modeled for a surface deposit of polonium. On the other hand, the FEP associated with a surface deposit is all but absent from samples doped with source solutions 247c and 247c', indicating the ^{210}Po was more successfully transported into the interior of the samples by this solution. These samples displayed multiple peaks at low energy, rather than a single peak corresponding to the expected fractional energy deposition value. In this section, spectra representative of surface and interior polonium deposits in gel-silica are presented. The author's interpretation of these spectra is provided, and implications of spectral features are discussed.

Surface Polonium Deposit. Figure 4-4 is an energy spectrum from a gel-silica sample doped with 20 μl of solution 247b and immersed in scintillation cocktail. The

modeled spectrum for a surface deposition of polonium is dashed in for comparison, and shows the excellent agreement between experiment and the modeled result. The continuum of counts between the peaks is an indication that the polonium deposit is not an ideal surface layer: these counts resulted from events where alphas originated a short distance inside the sample and ended their tracks in the bulk scintillation cocktail. The area under the FEP represents roughly 85% as many counts as the low energy peak, based on fits of Gaussian distributions to both peaks. This also agrees well with the expectation of equal peak areas for a surface deposit, especially considering that the continuum of counts between the peaks represent alphas heading out of the sample and should be included with the FEP counts for this comparison.

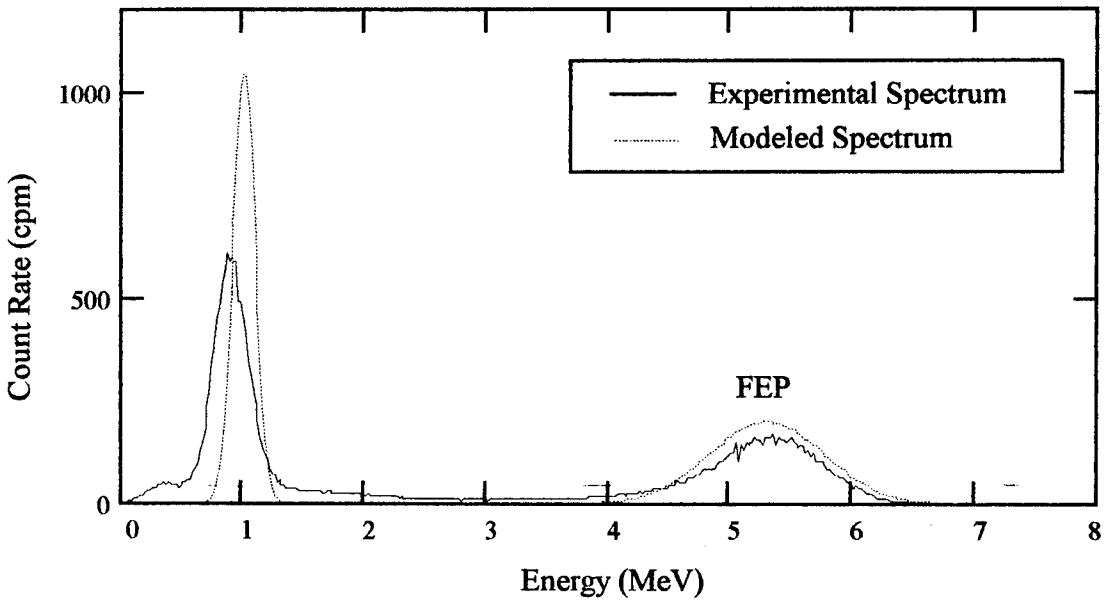

Figure 4-4. Comparison of experimental spectrum to that modeled for a surface deposit of Po210. The experimental data was calibrated based on the mean for the FEP falling at MCA channel 537.8. The modeled spectrum is based on a system resolution of 21% FWHM (representative of the resolution available on samples of Po210 in Ultima Gold), and was normalized to have the same area as the experimental spectrum.

The surface and near surface deposition of ^{210}Po which occurred when solution 247b was used agrees with the earlier discussion of the formation of colloids in that solution. Such colloids would not be drawn into the pore structure with the liquid, but rather would be filtered out at the surface. Also, dissolved polonium is expected to be rapidly adsorbed on silica from a basic solution (Figgins, 19: 1961), so that any ^{210}Po dissolved in the solution would not travel far into the pores before binding to the surface.

Although the agreement between modeled and experimental results seen in Figure 4-4 indicated that the sources of the two peaks are understood, verification of these interpretations was desired. In an attempt to isolate the low energy peak, the Ultima Gold was poured off the sample. This resulted in a gradual degradation of the FEP as cocktail on the external surfaces of the sample dried. Figure 4-5 depicts a spectrum taken 24.5 hours after the cocktail was poured off the sample. This spectrum shows slight degradation of the low energy peak, caused by decreased light collection efficiency which resulted from pouring off the liquid. The FEP was lost by this time, with a remnant of the counts which made up the FEP of Figure 4-4 appearing as a broad "peak" in the vicinity of 2 to 3 MeV. These counts are presumably due to alphas depositing energy in an Ultima Gold residue left on the surface of the sample.

Interior Polonium Deposit. Energy spectra from gel-silica samples doped with the acidic solutions indicate that the polonium was deposited within the pore structure, and show a transition over time which can be attributed to the migration of Ultima Gold into the pores. The peak expected at 1 MeV based on modeling is present in these spectra,

however appears to be transitioning into a higher energy peak. These features are discussed in the following paragraphs, with reference to the two time sequences of spectra shown in Figures 4-6 and 4-7.

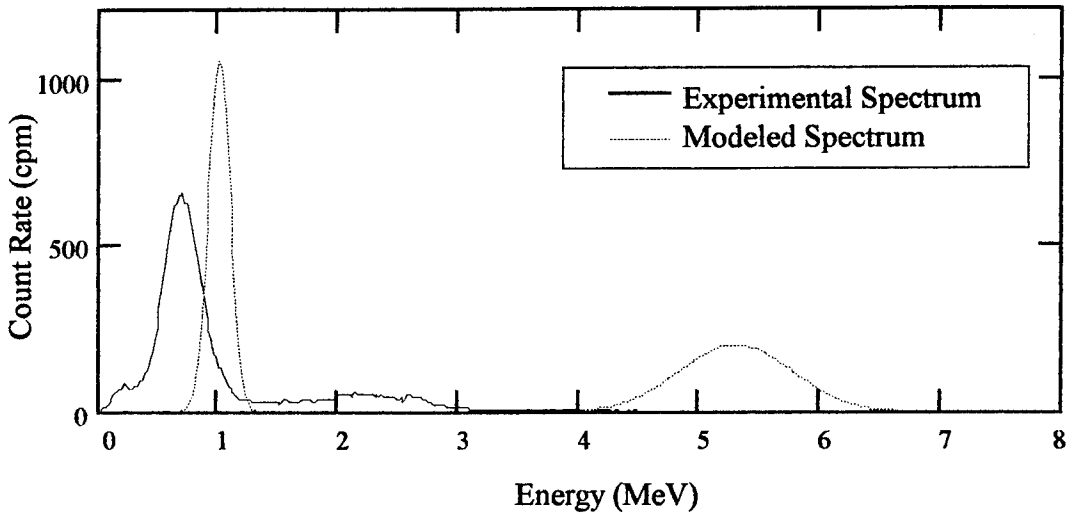

Figure 4-5. Energy spectrum taken one day after Ultima Gold was poured off a sample. Note loss of the FEP. The modeled spectrum from Figure 4-4 was carried forward for reference. Energy calibration used here is the same as that used in Figure 4-4.

The series of spectra presented in Figures 4-6 and 4-7 are time sequences taken from two samples doped with source solution 247c'. The times shown in each frame are referenced to the time of addition of Ultima Gold to the doped samples. The two samples progressed at different rates through the stages to be discussed below, likely due to the fact that one sample was initially protruding above the scintillation cocktail and the other was not. To facilitate the following discussion, the three peaks falling in the energy range from 0.5 to 2.5 MeV are designated as peak A (lowest energy), peak B, and peak C (highest energy).

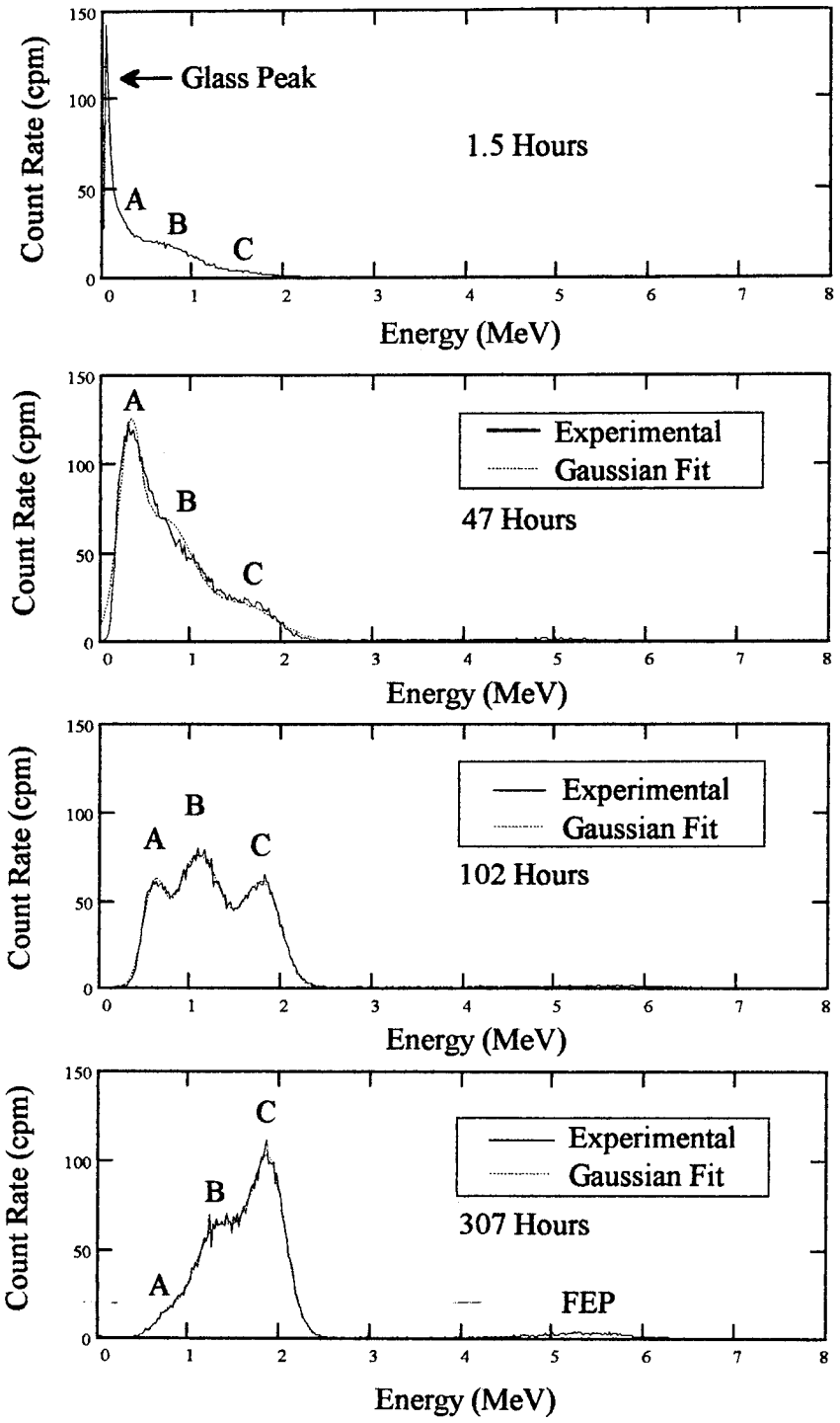

Figure 4-6. Time sequence of spectra from a gel-silica sample with an interior deposit of Po210. The sequence shows the transition which occurs as Ultima Gold fills the pores in the sample. Shown with fit of 3 Gaussian peaks to the composite peak between 0.5 and 2.5 MeV. Energy calibration based on the FEP in the lowest frame, with a mean falling at channel 550.

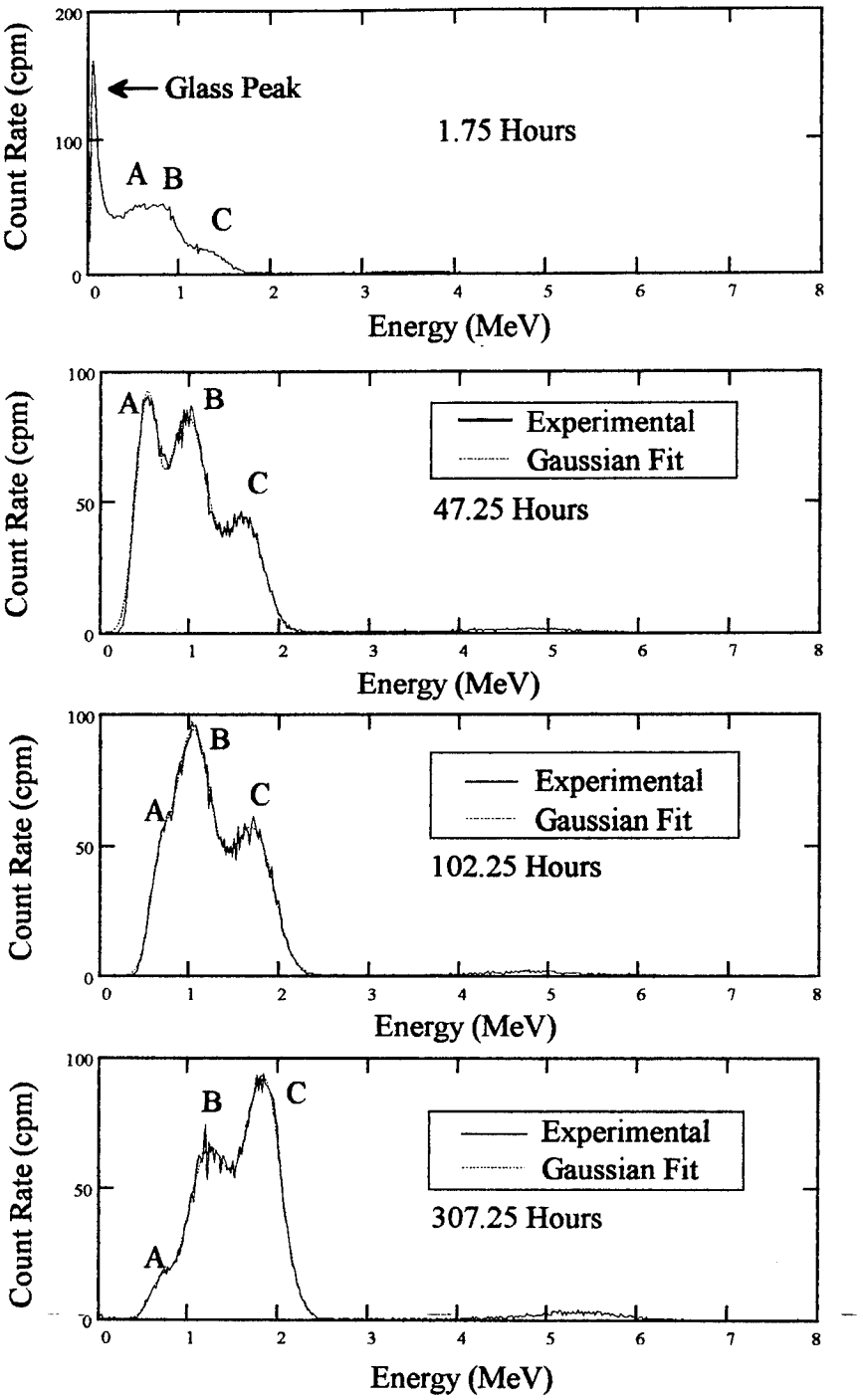

Figure 4-7. Second example of a time sequence of spectra from a gel-silica sample with an interior deposit of Po210. This sample transitioned more slowly than that of Figure 4-6. Shown with fit of 3 Gaussian peaks to the composite peak between 0.5 and 2.5 MeV. Energy calibration based on the FEP in the lowest frame, with a mean energy falling at channel 567.4.

The absence of an FEP in the top frames of Figures 4-6 and 4-7 indicates that the polonium added to these two samples was deposited within the pore structure, rather than at or near the exterior surface of the samples. The gradual increase in counts in the FEP location over time indicates that diffusion of a small amount of polonium out of the samples occurred over the 13 days represented in these sequences.

Most of the changes seen in the structure of the spectra of Figures 4-6 and 4-7 can be attributed to the movement of liquid scintillant into the pores of the gel-silica samples. Three of the peaks can be readily explained, and one plausible cause for peak C is postulated.

Glass Peak. The low-energy peak seen in the top frame of both figures was created by alpha particles causing scintillations in the glass in regions of the matrix where the liquid had not yet penetrated. The counts registered at energies above that of the glass peak were caused by alphas transiting regions where the scintillant had reached, and represent the composite of peaks A, B, and C which emerge more prominently in subsequent frames. The glass peak is gone by the second frame, indicating that at least some scintillant is within range of all alpha particles emitted within the sample. This conclusion is based on the fact that energy deposited in the glass would be detected coincidently with energy deposited in liquid scintillant, so counts that would fall in the glass peak are boosted to a higher energy if they encounter liquid scintillant.

Peak A: Transition. The prominence of peak A in the second frame of each figure, along with the absence of the glass peak, suggest that a network of the most accessible pores filled with liquid while surrounding pores remained unfilled. In this

situation, alphas could encounter scintillant along their tracks, however not deposit as much energy as they would traveling through a fully filled pore structure. The mean energy of this peak is seen to increase in energy with time, which agrees with the idea of a region gradually filling outward from the initial network of filled pores. The lower two panels of both figures show peaks B and C increasing in area at the expense of peak A, consistent with the concept that peak A is a transitional peak which would lose counts to peaks B and C as the pore structure became filled with liquid.

Peak B: Energy Deposition in Filled Pores. Peak B falls very near 1 MeV, the modeled energy value for the detection of 5.304 MeV ^{210}Po alphas in 30% porous gel-silica filled with Ultima Gold liquid scintillant. The presence of this peak supports the modeling results. By the bottom frame in Figures 4-6 and 4-7, it appears that peak B is losing counts to peak C, as well as transitioning to higher energies. This would not be expected based on the movement of liquid scintillant alone, if peak B does indeed represent the energy alphas deposit in the liquid phase when the pore structure is filled. One possible explanation for this transition is discussed in the next paragraph.

Peak C. The transition sequence depicted in Figures 4-6 and 4-7 may ultimately end with only Peak C (and the FEP) present, as the transition was apparently not complete as of this writing. The most straightforward explanation for this peak is that it represents the final value for fractional energy deposition in the Ultima Gold filled pores, i. e. that the transition from peak B to peak C results from the filling of additional pores (perhaps a smaller range of pore dimensions). However, the 1.8 MeV energy of this peak

does not agree with the 1 MeV modeled for energy deposition in Ultima Gold filling 30% porous gel-silica. Without the presence of peak B during the transition, this would necessarily be taken to indicate problems with the modeling effort. This conclusion is held at bay by the agreement between the energy of peak B and the modeled result, which suggests that an additional factor is coming into play in the transition to Peak C. Several possibilities have been considered, however the data available at present do not allow a definitive conclusion. It is likely that peak C was caused by the presence of stress fracture zones within the material, caused by the stresses induced by hydration of the samples. To be consistent with the modeled results of Chapter 3, such an explanation would require that the resultant porosity of the material be increased up to the vicinity of 50% in the region of a fracture zone (see Figure 3-7). Also, the transition of counts from peak B into peak C may suggest that new fracture zones form during the transition period.

The time sequences of spectra shown in Figures 4-6 and 4-7 represent a valuable look at the movement of liquid scintillant into the pore structure of gel-silica, as well as an indication that diffusion information could be gained as polonium moves out of the sample and into the bulk scintillation cocktail. Transitions in the glass peak and peak A are readily explained on the basis of movement of the scintillant into the pore structure. Peak B corresponds well to the modeled value of 1 MeV which should be deposited into the liquid phase when these samples are filled with Ultima Gold. The cause for transfer of counts into peak C is not fully understood, however this peak may represent alpha particles depositing more than the expected amount of energy into the liquid phase by transiting fracture zones caused by hydration of the samples.

Detection Efficiency in Gel-silica. Detection efficiencies were calculated for five measurements made on a sample doped with solution 247c, and for three measurements each on two samples doped with solution 247c'. All counts recorded in the first 1000 channels of the MCA, after background subtraction, were summed to determine the total count (the same method as used to calculate the known specific activity of the source solutions). Table 4-4 contains the results of these measurements. The average of these measurements, weighted by their respective uncertainties (Bevington, 59: 1992) yields a detection efficiency of 99.0(1.0)%, which is in excellent agreement with the 100% detection efficiency expected.

Table 4-4. Detection Efficiency Data

Sample	Source Solution	Mass of Doping Solution(mg)	Corrected Mass (mg)	Count Rate (cpm(2σ))	Known Activity (dpm)	Efficiency (%)
Po14	247c	16.76(0.07)	18.0(0.5)	97.5(2.7)	95.1(2.7)	102.5(4.2)
"	"	"	"	96.9(2.7)	95.0(2.7)	102.0(4.2)
"	"	"	"	94.3(2.7)	93.6(2.7)	100.7(4.1)
"	"	"	"	90.8(2.7)	89.5(2.6)	101.3(4.2)
"	"	"	"	86.1(1.1)	86.5(2.5)	99.5(3.1)
Po22	247c'	8.76(0.05)	9.42(0.26)	5140(37)	5200(150)	98.7(3.0)
"	"	"	"	5096(37)	5150(150)	99.0(3.0)
"	"	"	"	4931(36)	4930(150)	100(3.1)
Po23	247c'	9.01(0.05)	9.69(0.26)	5165(37)	5350(160)	96.5(2.9)
"	"	"	"	5087(37)	5290(160)	96.1(2.8)
"	"	"	"	4928(36)	5070(150)	97.2(2.9)

See Appendix C for a discussion of the mass correction.

Energy Resolution in Gel-silica. Several factors exist that may cause broadening of energy peaks in the detection of alpha particles within gel-silica, yet some samples provided peaks which were only slightly less resolved than those measured in bulk scintillation cocktail. The most likely cause for broadening of the energy peak is a non-uniform loading of the pores with scintillant (Hench *et al*, 2: 1993), a situation which would increase the spread in energies deposited in the pores. The use of gel-silica with larger pore dimensions may mitigate this problem. Further, if a scintillating gel-silica is produced there should be less difficulty in achieving uniform filling of the pores with aqueous samples. Another possible contributor to the energy peak width is the scattering of scintillation light from phase interfaces within the sample. Such scattering causes the scintillation light to travel longer path lengths prior to escaping the sample, leading to increased absorption of scintillation light within the sample. Non-uniform light collection efficiency caused by the irregular geometry of the samples may also contribute to the energy peak width. Despite these potential pitfalls, the best energy resolution observed for the detection of alpha particles inside a gel-silica sample was 23.7% FWHM (observed for peak C in Figure 4-6). This resolution is only slightly poorer than the 21% which was generally observed for samples of polonium measured in scintillation cocktail. This result is significant, as it shows only slight degradation of the resolution despite the presence of the heterogeneous gel-silica and Ultima Gold matrix.

The modeled value of intrinsic energy resolution for the gel-silica and Ultima Gold matrix is significantly better than the resolutions achieved experimentally, however a comparison cannot be made between these data and the modeled result. A system with

system resolution on the order of the expected intrinsic resolution will be required to test the validity of the model predictions for intrinsic energy resolution.

Detection Efficiency in Glass Bead and Liquid Scintillator Matrix. In the following experiments, the difference in detection efficiency for adsorbed and volume distributed emitters at large sphere size was probed.

Transition from Volume to Surface Distributed Radionuclides. The first experiment consisted of doping 300 μl of Ultima Gold with a 10 μl drop of solution 247c'. This vial was counted to establish the ^{210}Po activity contained, then 1.00 gram of glass beads were added and the vial was recounted. A series of counts ensued to see if changes in the detection efficiency and energy spectra occurred with time. The hope was that the polonium would be distributed through the volume of the scintillator initially, and adsorb onto the glass over time. The measurable effect would be a drop in detection efficiency with time, as well as emergence of a low energy peak in the energy spectra associated with alphas detected solely in the glass. Detection efficiencies and energy spectra obtained from this experiment are presented below.

Data taken according to the discussion above is shown in Table 4-5, along with the calculated detection efficiencies. The detection efficiency is also presented graphically as a function of time in Figure 4-8. These data show that the detection efficiency was initially high, and declined over time. The initial 15 minute count taken after the beads were added had a 97.6(1.0) % counting efficiency. This result agrees very well with the 100% efficiency modeled, particularly considering that some counts would

be lost due to degradation of the energy spectrum by poor light collection efficiency. By the last count taken, the efficiency had dropped to 91.4(1.0) %. This drop, although not as drastic as expected if all the polonium were on the surface of the beads, shows qualitative agreement with the model expectations. It is likely that an equilibrium was reached with only a fraction of the polonium adsorbed onto the beads. Such a situation would result in a higher efficiency than that modeled for a completely adsorbed source.

Table 4-5. Detection Efficiency Data

Time (hours)	Count Rate (cpm(2σ))	Detection Efficiency (%)	Comments
0	5411(38)	100	Prior to addition of beads
0.33			Beads added
0.55	5280(37)	97.6(1.0)	
1.75	5187(37)	95.9(1.0)	
2.4	5112(19)	94.5(0.8)	
4.25	5085(18)	94.0(0.8)	
6	5028(18)	93.0(0.8)	
7.7	5019(18)	92.9(0.8)	
9.5	5004(18)	92.7(0.8)	
11.2	4983(18)	92.3(0.8)	
12.9	4994(18)	92.5(0.8)	
14.7	4971(18)	92.1(0.8)	
16.3	4957(18)	91.9(0.8)	
38.8	4906(18)	91.4(1.0)	

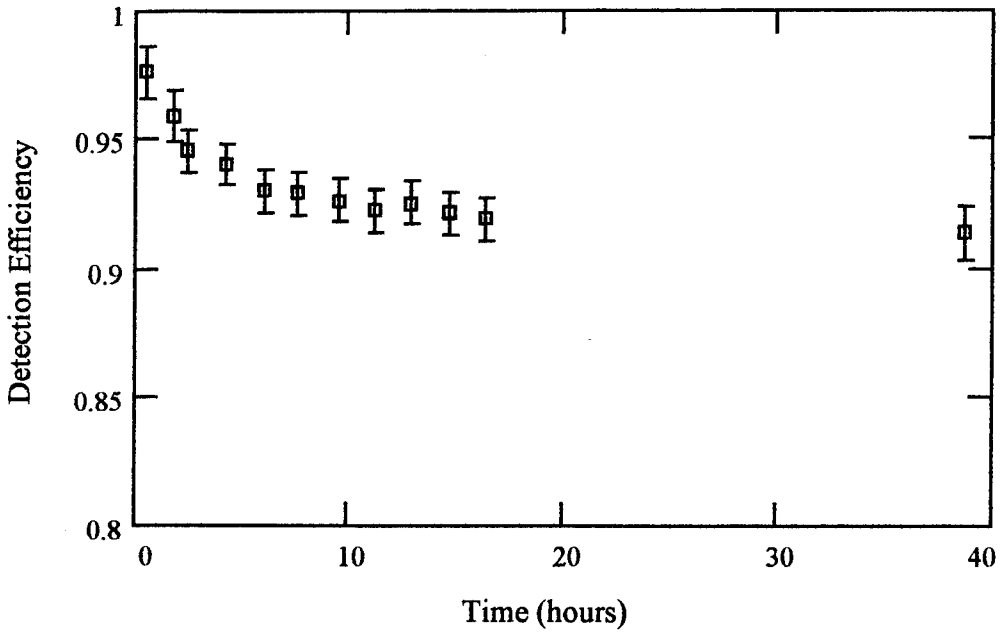

Figure 4-8. Drop in detection efficiency observed as polonium adsorbed onto glass beads.

The time sequence of energy spectra shown in Figure 4-9 shows the transition which occurred after the glass beads were added to the doped Ultima Gold. The top spectrum shows the alpha FEP obtained just prior to addition of the beads. The next spectrum in the sequence represents a 15 minute count started 5 minutes after the glass beads were added. The immediate degradation of the spectrum is apparent, and can be attributed to alpha energy loss in the glass beads (see Figure 3-14) and to increased scatter leading to absorption of scintillation light in the matrix. A feature absent from this frame is the low energy peak associated with scintillation in the glass. This indicates that the majority of the polonium was distributed through the liquid during this count, so that light generated in the glass is coincident with light generated in the liquid for each alpha which strikes a bead, and the glass peak is not seen. 135 minutes after the beads were added

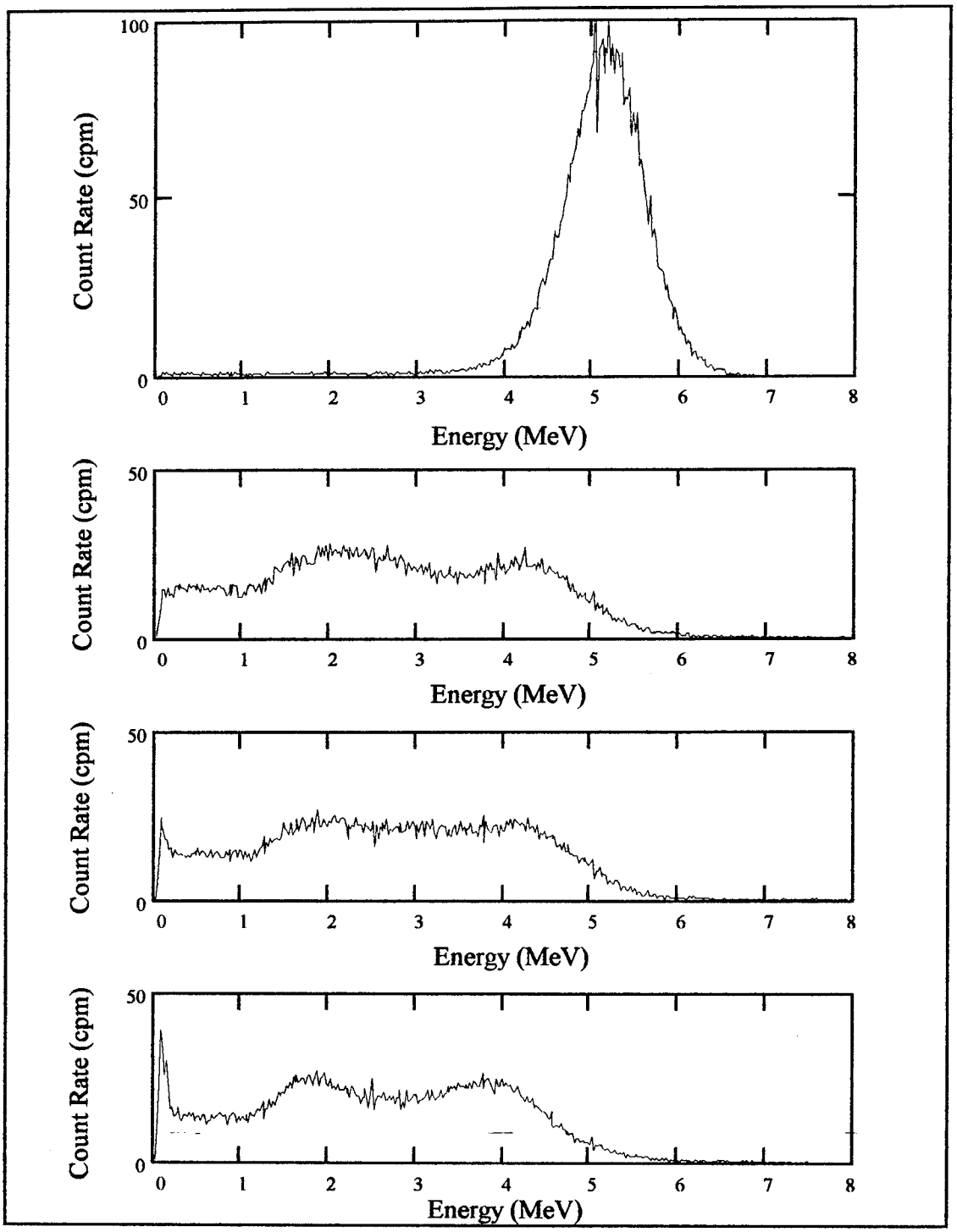

Figure 4-9. Transition of Po210 energy spectrum due to addition of glass beads and subsequent adsorption of polonium onto the beads. The energy scale was calibrated based on the FEP in the top frame, with a mean falling in channel 524.2.

enough polonium had adsorbed to the spheres to form the glass scintillation peak, as shown in the third spectrum displayed in Figure 4-9. Continued growth of the peak occurred, as shown in the last spectrum taken 38 hours after addition of the beads.

Polonium Adsorbed on Glass Beads. In this experiment the intent was to ensure that the polonium was on the surface of the beads, so the efficiency for detection in the adsorbed case could be determined. To do so, 1.01 grams of beads were doped with solution 247c' and dried. Five minutes after addition of Ultima Gold, the 15 minute count which yielded the upper spectrum shown in Figure 4-10 was started. The glass peak at low energy attests to the presence of polonium on the surfaces of the glass beads. Without the glass peak, the shape of this spectrum is in excellent agreement with the modeled result (Figure 3-14). The FEP appears at less than half of the expected 5.304 MeV, an effect once again attributed to the reduction in light collection efficiency due to addition of the beads. The detection efficiency calculated for this count is 79.1(1.2)%. If the glass peak is artificially truncated as shown in the lower half of Figure 4-10, this efficiency drops to 70%. This value represents an estimate of the efficiency for detection of alphas adsorbed to the surface of the glass beads. Although this value is still significantly higher than the 57.2 % modeled value, it represents additional support for the validity of the results from Alpha.bas. It is likely that some of the polonium was brought into solution almost immediately after the cocktail was added, which would result in a higher detection efficiency than the result modeled assuming all of the polonium is on the surface of the beads.

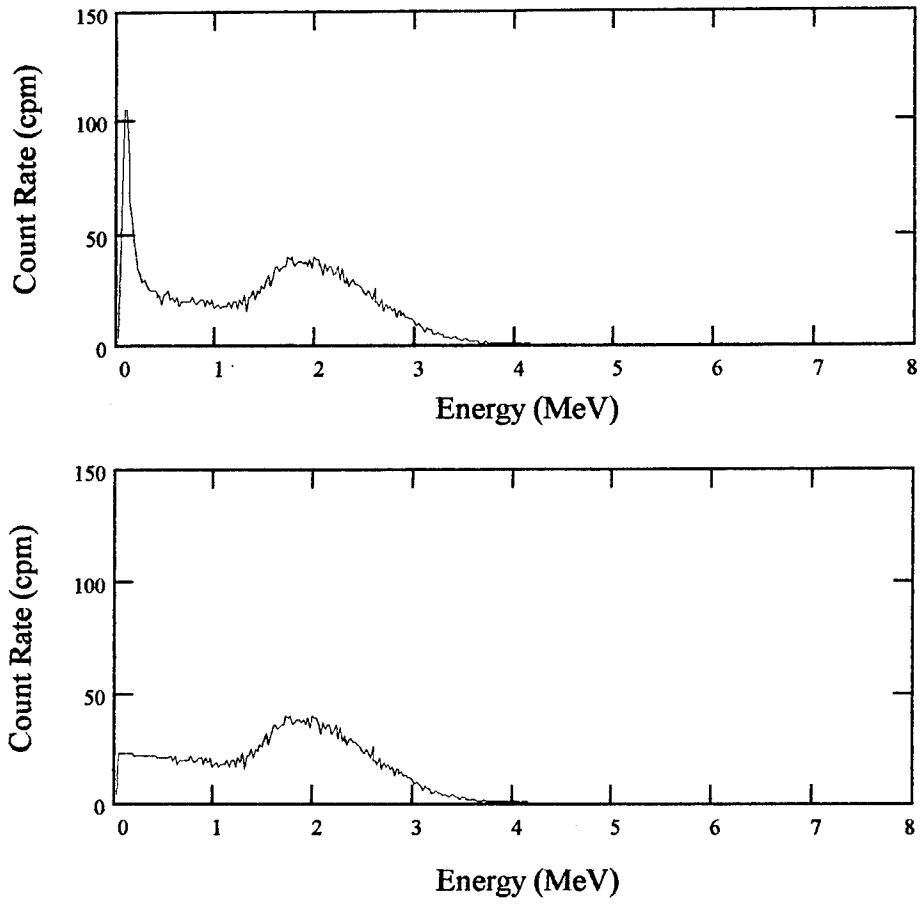

Figure 4-10. Energy spectrum obtained from a sample of glass beads with most of the Po210 adsorbed on the surfaces of the beads (top). The lower spectrum is the same spectrum with the glass peak artificially truncated to estimate the count rate attributed to detection in the liquid phase. The energy scale was calibrated based on the peak in the top frame of Figure 4-9.

The data collected during the experimental portion of this project support the modeling results presented in Chapter 3. Energy peaks associated with the deposition of energy in the liquid phase of gel-silica and liquid scintillator are in agreement with the modeled value. The alpha detection efficiency in gel-silica was measured as 99.0(1.0)%, in excellent agreement with the 100% expected. Detection efficiencies measured in a glass

bead and liquid scintillator matrix were found to be in qualitative agreement with the model. The ideal distributions of polonium, either on the surface of the beads or uniformly distributed through the liquid scintillator, were likely not achieved, leading to the quantitative differences between the modeled and experimental results. The conclusions and recommendations which can be drawn from the modeling and experimental work completed for this project will be presented in the next chapter.

V. Conclusions and Recommendations

Conclusions

The conclusions drawn from this project are presented below. Unless otherwise specified, each conclusion applies to alpha particle detection in heterogeneous scintillation detectors with one active phase which can be reasonably modeled by the FCC structure. These conclusions do not necessarily apply to detectors where one of the phases is a gas.

Validity of the Model. Output from Alpha.bas provides valid estimates for the partition of energy between phases of the detector, the geometric detection efficiency for alpha particles, and the intrinsic energy resolution for proposed detector materials. Results for a specific material, for instance the maximum phase dimension which will provide a required intrinsic energy resolution, are material dependent and must be simulated individually. The following general conclusions can be made based on modeling results.

Alpha Detection Efficiency.

1. 100% geometric efficiency for alpha particle detection is achieved as the dimensions of the phase regions in the detector become small compared to the alpha range in the detector.

2. The geometric detection efficiency decreases more rapidly with increasing particle size for emitters distributed through the inactive phase of the detector than it does for emitters adsorbed on the surface of the active phase.

Intrinsic Energy Resolution. The intrinsic energy resolution of a detector will significantly degrade system resolution if the scintillating and non-scintillating phase regions have dimensions comparable to the alpha range in the detector. Generally, intrinsic resolution improves with decreasing phase region dimensions. An exception to this occurs for adsorbed emitters, where most events result in full alpha energy deposition in one or the other phase at large particle sizes.

Alpha Detection in Gel-silica. The following conclusions concerning gel-silica are made based on the modeling and experimental results presented in previous chapters.

1. Gel-silica filled with liquid scintillant can provide 100% detection efficiency for alpha particles emitted within the pore structure. The same can be expected if a scintillating gel-silica is developed.

2. The detection efficiency for radionuclides at the exterior surface of a gel-silica detector will be significantly reduced from 100% if the cell is surrounded by a non-scintillating material. This may impact the efficiency for detection of radionuclides which have a strong affinity for the silica surface, and are adsorbed at the exterior surface before entering the pore structure of the flow cell.

3. The changes observed in energy spectra for alpha emitters deposited within gel-silica provide information on the diffusion of materials into and out of the gel-silica matrix. Spectral features and temporal evolution of these features may also provide insight into the internal structure of gel-silica, for instance by indicating the presence of fracture zones within the material.

4. Alpha particle energy is partitioned between the phases in a liquid filled gel-silica. It does not appear that significant energy transfer from the glass to the fluors in the liquid phase occurred in the experimental work reported here.

5. Equation 3-11, based on the Bragg-Kleeman approximation for the ratio of alpha ranges in two media, can be used for a reasonable estimate of the partition of alpha energy between the phases of liquid filled gel-silica.

6. Good collection of scintillation light generated within gel-silica can be achieved.

Flow Cell Design.

1. Gel-silica has promising potential for incorporation into a flow cell alpha spectroscopy system.

2. Stress fracturing may significantly alter the energy spectra of alpha particles detected in gel-silica. This is an undesirable trait in an alpha spectroscopy system.

3. The fractures observed in gel-silica samples used in this work indicate that materials with pore dimensions larger than the 2.0 nm tested may be required to improve stability to water diffusion.

4. The system energy resolution of a system relying on backfill of liquid scintillation cocktail into gel-silica will be significantly degraded if the scintillant is not loaded uniformly into the pores.

5. The long time frame over which scintillant moved into the 2.0 nm gel-silica pore structure indicate that a system relying on backfill of liquid scintillant may be impractical. Larger pore dimensions may mitigate this problem to some extent.

6. An alpha spectroscopy system built around a flow cell designed to accumulate radionuclides of interest on large size scintillating particles may be possible. However, the detection efficiency would be on the order of 50% in this case, and the available surface area may not permit high collection efficiencies. Scattering and self absorption of scintillation light is likely to further degrade system performance in this type of design.

7. Alpha spectroscopy systems should not be designed to incorporate scintillating particles with radii of the same order of magnitude as the alpha range in the detector without consideration of the poor intrinsic energy resolution which will result.

Recommendations

Scintillating Gel-silica. Efforts to develop a scintillating gel-silica should be continued. Possible benefits of including a wavelength shifter should also be considered. As mentioned in the conclusions, it seems likely that a system relying on backfilling gel-silica with scintillation cocktail will be impractical. Thus, development of a scintillating gel-silica may be critical to the success of designing an alpha spectroscopy flow cell utilizing gel-silica.

Liquid Scintillant and Gel-silica. Research relying on incorporation of liquid scintillant into gel-silica should be continued.

PERALS. PERALS methods should be applied to alpha spectroscopy in gel-silica. PERALS has provided alpha energy resolutions on the order of 5% and should allow significant improvement over the resolutions reported here. This would involve a variety of changes from the methods reported in this paper, including: 1) incorporating pulse shape discrimination methods to distinguish pulses caused by alphas from those caused by beta and gamma radiation, 2) use of scintillation cocktail designed specifically for alpha work, and 3) use of detector designs which have been optimized for alpha particle detection.

Diffusion Studies. Diffusion studies based on the diffusion of materials into and out of the pore structure of gel-silica are possible.

Fluorescence Lifetimes. The small dimensions of gel-silica pores represent the opportunity to study the effects of confinement on the fluorescence lifetimes of fluors introduced into the gel-silica matrix.

Detection of Beta Emitters. The detection of beta radiation in gel-silica should be pursued. High detection efficiencies for low energy beta emitters, for instance ^{3}H, may be possible.

Larger Pore Sizes. Gel-silica with larger pore sizes should be studied to determine if liquid scintillant can be more rapidly incorporated into the matrix.

Alpha Spectroscopy System Development. Successful development of an alpha spectroscopy, alpha-gamma coincidence flow cell detector utilizing gel-silica requires research in the following areas:

Flow Rates and Backpressure. The dependence of water flow rates and backpressures on gel-silica porosity and pore size must be determined to allow selection of a gel-silica capable sufficient flow rates within the operating pressures of commercially available pumps.

Collection Efficiencies. The collection efficiencies for adsorbing radionuclides of interest within gel-silica must be determined. Further, the dependence of these efficiencies on pH and surface modifications are of interest.

Alpha-Gamma Coincidence. Alpha-gamma coincidence should be studied. ^{235}U has a high coincidence yield and should be a good nuclide to use for initial experimental work. ^{224}Ra and ^{226}Ra should then be studied to determine if their low coincidence yields are sufficient to differentiate them from ^{222}Rn and ^{234}U, respectively.

Other Methods to Separate Nuclides. Other methods to identify specific nuclides, within the framework of the system concept, should be found. For instance, if ^{234}U has a high collection efficiency within gel-silica, the flow cell might be flushed with clean water immediately prior to a count to remove interfering ^{222}Rn from the cell.

Appendix A: Code Alpha.bas

```
DECLARE SUB EnergyInterp ()
DECLARE FUNCTION EnergyLeft# (material%, residualrange#)
DECLARE SUB PICKCOORDADSORBED ()
DECLARE SUB PICKCOORD ()
DECLARE SUB COMBINEDATA (k%)
DECLARE SUB EXITCUBEPOINT (XI#, YI#, ZI#, range#)
DECLARE SUB INTERSECTIONS (XI#, YI#, ZI#, A#, B#, C#, D#, E#, F#)
DECLARE SUB ADDVECTOR ()
DECLARE SUB SPHERESEQUENCE ()
DECLARE SUB WHEREISIT (XF#, YF#, ZF#, InLeavesEnergy%, OutLeavesEnergy%)
DECLARE FUNCTION CALCRANGE# (energy#, material%)
DECLARE SUB EDEP (pcntrangeto1#, pcntrangeto2#, edepinsphere#, WHICHSPHERE%)
DECLARE SUB NORMVECTOR (VX#, VY#, VZ#, length#)
DECLARE SUB CHANGEVAR ()
DECLARE SUB VARLIST ()
DECLARE SUB BEEP1 ()
DECLARE SUB BEEP2 ()
DECLARE SUB HELLO ()
DECLARE SUB INITVAR ()
DECLARE SUB PICKVECTOR ()
DECLARE SUB USERINPUT ()
DECLARE SUB SPHERE (WHICHSPHERE%, D#, E#, F#, edepinsphere#)
DECLARE SUB VARSUMMARY ()
DECLARE FUNCTION FITSPHERES# (X#, Y#, Z#)
DECLARE SUB MOVETONEXTCUBE (XI#, YI#, ZI#)
DECLARE SUB ENERGYDEPOSITION (residualrange#, edepinsphere#)
DECLARE SUB WRITTENSUMMARY (InLeavesEnergy%, OutLeavesEnergy%)
'
'Program Alphas.bas
version$ = "Alpha Ver 1.01"
'
'  This program is written in QBasic for use on a PC.  It was modified
'by Martin Keillor from the code Alpha Detector(copyright 1988) written
'in TurboPascal by H.H. Ross and L.L. Rozevink.  Simulations will benefit
'from using a fast machine and a numeric coprocessor.  The authors reserve
'the right to modify the code at any future time without notification.
'This source code may be used freely with acknowledgement.
'
'  Questions related to the code should be directed to:
'
'  Dr. H. H. Ross                    Dr. L. Burggraf
'  Oak Ridge Nationel Laboratory     Air Force Institute of Technology/ENP
'  P.O. Box 2008                     2950 P Street
'  Oak Ridge, TN 37831               Wright-Patterson AFB OH 45433-7765
'
DEFDBL A-Z
DEFINT I-K
DIM pcntrangeto1(1 TO 14)
DIM pcntrangeto2(1 TO 14)
```

```
DIM SEQUENCE%(1 TO 5)
DIM SHARED CENTERS(1 TO 14, 1 TO 3)
DIM SHARED RangeTable(2, 20)
'
'*************************************************************************
'                                                                        *
'*                    VARIABLE DICTIONARY                               *
'*                                                                      *
'*                                                                      *
'* A, B, C. . . . . .          Values used in the quadratic eqn in      *
'*                             SUB INTERSECTIONS                        *
'* AdsorbedFlag%. . . . . .    Boolean variable which indicates user    *
'*                             preference for adsorbed or volume        *
'*                             distributed alpha emitters               *
'* answer$. . . . . .          Hold user response to prompts            *
'* Centers. . . . . .          Array containing the coordinates of      *
'*                             the 14 spheres in the FCC unit cell      *
'* code%. . . . . .            Hold user response to prompts            *
'* Const1, 2, 3 . . . . . .    temporary variables used to reduce       *
'*                             line lengths                             *
'* Criteria1, 2, 3, 4 . . . . . .  Boolean variables for various        *
'*                             geometric test criteria                  *
'* density. . . . . .          Accepts user input value for the         *
'*                             density(g/cm^3) of the material          *
'*                             between the spheres                      *
'* densitysphere. . . . . .    Ditto for the sphere material            *
'* DetAsLightCount% . . . . . .  Number of alphas detected for a given  *
'*                             radius                                   *
'* DetEfficiency. . . . . .    The modelled detection efficiency        *
'* Discriminator. . . . . .    Used to determine if an alpha            *
'*                             deposits enough energy to be detected    *
'* DistanceThroughSphere. . . . . .  Distance through the sphere along the *
'*                             alpha track                              *
'* DistanceToSide . . . . . .  Distance to the side of the unit cell    *
'*                             from the alphas initial point            *
'* AePore . . . . . .          Accepts user input value for the         *
'*                             effective atomic mass of the material    *
'*                             between the spheres                      *
'* AeSphere . . . . . .        Ditto for the sphere material            *
'* edepinsphere . . . . . .    Tracks energy deposited in spheres by    *
'*                             an alpha                                 *
'* Energy . . . . . .          Alpha energy in MeV                      *
'* EnergyOut$ . . . . . .      Filename for output of energy            *
'*                             deposited in spheres for each event      *
'* events%. . . . . .          Tracks the number of events which        *
'*                             remain to be simulated (for a given      *
'*                             radius)                                  *
'* ExitSide%. . . . . .        Side of the unit cell the alpha exits    *
'* factor1, 2 . . . . . .      Temporary variables used to reduce       *
'*                             line lengths                             *
'* fraction . . . . . .        Fraction of a range interval in the      *
'*                             RangeTable.  Used for linear interp      *
```

```
'* GoodIP . . . . . .    Boolean used to signify a generated      *
'*                       point is within the unit cell            *
'* Goodpoints%. . . . . .  Maintains the number of events to be    *
'*                       simulated                                *
'* InCubeInSphere . . . . . .  Counts number of alphas which end in *
'*                       the unit cell and in a sphere            *
'* InLeavesEnergy . . . . . .  Counts number of alphas which end in *
'*                       the unit cell and deposit energy in a    *
'*                       sphere                                   *
'* Intercepts . . . . . .   # of intersections of the alpha track   *
'*                       with a given sphere                      *
'* InVoidVol. . . . . .     Counts number of alphas which end in    *
'*                       the interstitial without exiting the     *
'*                       initial unit cell                        *
'* index. . . . . .         Loop control variable                   *
'* InfoFile$. . . . . .     Filename for output of user entered     *
'*                       parameters.                              *
'* i, j, k. . . . . .       Loop control variables                  *
'* L. . . . . .             Coordinate for sphere centers           *
'* length . . . . . .       Desired magnitude of a vector passed    *
'*                       to SUB NORMVECTOR                        *
'* LongRangeFlag% . . . . . .  Boolean flag which indicates if the  *
'*                       alpha has moved beyond a unit cell       *
'* loopflag%. . . . . .     Loop control variable                   *
'* MasterCounter% . . . . . .  Tracks total number of initial points *
'*                       generated for each radius                *
'* minenergy. . . . . .     Accepts user input value for the        *
'*                       minimum energy required for detection    *
'*                       Currently commented out and set to 0     *
'*                       (geometric efficiency)                   *
'* norm . . . . . .         Magnitude of a vector                   *
'* NotCubeInSphere. . . . . .  Counts number of alphas which end    *
'*                       outside of the unit cell but in one      *
'*                       of the 14 spheres associated with the    *
'*                       initial unit cell                        *
'* OutLeavesEnergy% . . . . . .  Counts number of alphas which end  *
'*                       outside the unit cell and deposit        *
'*                       energy in a sphere                       *
'* OutputFile$. . . . . .   Accepts user input for output           *
'*                       filename.  3 files are created, using    *
'*                       this string appended with ".inf",        *
'*                       ".prn", and "r.prn"                      *
'* pcntrangeto1, 2. . . . . .  Vector of ranges to sphere surfaces  *
'*                       (% of remaining range).  Also used       *
'*                       as a single valued variable to hold      *
'*                       a % range in SUB EDEP                    *
'* porosity . . . . . .     Accepts user input value for the        *
'*                       porosity (volume of interstitial /       *
'*                       total volume) Default is FCC porosity    *
'* range. . . . . .         Range of the alpha (cm).  This          *
'*                       variable is decremented as the alpha     *
'*                       loses energy                             *
```

```
'* RangeAir . . . . . Range of an alpha in air                    *
'* RangeSave. . . . . Stores the range of the full energy         *
'*                    alpha in the interstitial material          *
'* RangeSolid . . . . . Range in the sphere material left         *
'*                    to an alpha entering a sphere               *
'* RangeTable . . . . . Array used to store range vs. energy      *
'*                    values for air and the two materials        *
'*                    (sphere and interstitial)                   *
'* ResEnergyLiquid. . . . . Energy remaining to an alpha as it    *
'*                    exits a sphere                              *
'* ResEnergySolid . . . . . Energy remaining to an alpha as it    *
'*                    enters a sphere                             *
'* residualrange. . . . . Range remaining to the alpha in the     *
'*                    interstitial material                       *
'* ResRangeSolid. . . . . Range in the sphere material left       *
'*                    to the alpha as it exits a sphere           *
'* Sequence . . . . . equence of spheres the alpha                *
'*                    encounters                                  *
'* steps% . . . . . User supplied number of radius                *
'*                    increments                                  *
'* time . . . . . Array used in SUB EXITCUBEPOINT to              *
'*                    determine which side of the unit cell       *
'*                    the alpha exits (psuedo - time)             *
'* timetoside . . . . . Shortest time for alpha to reach a        *
'*                    side of the unit cell (psuedo-time)         *
'* TemporaryFile$ . . . . . Temporary filenames used by program   *
'* transfer . . . . . Temporary variable used in SUB              *
'*                    COMBINEDATA to transfer data from one       *
'*                    file to another                             *
'* VX, VY, VZ . . . . . Vector components representing            *
'*                    direction of alpha travel                   *
'* WhichSphere% . . . . . Informs certain SUBS/FUNCTIONS which   *
'*                    of the 14 spheres is being considered       *
'* XF, YF, ZF . . . . . Final coordinates of alpha                *
'* XI, YI, ZI . . . . . Initial coordinates of alpha              *
'* Xvector, Yvector, Zvector. . . . Vector components used in generation *
'*                    of a random point on a sphere               *
'*************************************************************************
CLS
COLOR 15, 9
CALL BEEP1
CALL HELLO
COLOR 15, 0
CLS
pi = 4 * ATN(1)
CALL USERINPUT
CALL CHANGEVAR
CALL EnergyInterp
RangeSave = CALCRANGE(energy, 2)
GoodPoints% = events%
FOR k = 0 TO steps%
   CALL INITVAR
```

```
    IF k < 10 THEN
       TemporaryFile$ = "EDEP" + RIGHT$(STR$(k), 1) + ".dat"
       ELSE
          TemporaryFile$ = "EDEP" + RIGHT$(STR$(k), 2) + ".dat"
    END IF
    OPEN TemporaryFile$ FOR OUTPUT AS #2
    RANDOMIZE TIMER
    CALL VARSUMMARY
    PRINT
    CALL BEEP1
    '
    PRINT "CALCULATING ------------------------->"
    PRINT
    DO
       range = RangeSave   'Reset range value
       IF AdsorbedFlag% THEN
          CALL PICKCOORDADSORBED
          ELSE
             CALL PICKCOORD
       END IF
       CALL PICKVECTOR
       CALL NORMVECTOR(VX, VY, VZ, range)
       CALL ADDVECTOR
       CALL WHEREISIT(XF, YF, ZF, InLeavesEnergy, OutLeavesEnergy%)
       events% = events% - 1
       PRINT "DOWN TO:"; events% + (steps% - k) * GoodPoints%
    LOOP UNTIL events% = 0
    COLOR 15, 9
    CLS
    CALL BEEP2
    CALL WRITTENSUMMARY(InLeavesEnergy, OutLeavesEnergy%)
    PRINT
    CLOSE #2
    radius = radius + stepsize
    events% = GoodPoints%
NEXT k
COLOR 15, 9
CLOSE
CALL COMBINEDATA(steps%)
END

SUB ADDVECTOR
'
' THIS PROCEDURE ADDS THE VECTOR COMPONENTS ONTO THE CORRESPONDING
' INITIAL COORDINATES
'
    SHARED XF, XI, VX, YF, YI, VY, ZF, ZI, VZ
    XF = XI + VX
    YF = YI + VY
    ZF = ZI + VZ
END SUB
```

```
SUB BEEP1 STATIC
' THIS PROCEDURE ENABLES THE COMPUTER TO AUDIBLY SIGNAL THE USER WHEN
' CERTAIN PORTIONS OF THE PROGRAM HAVE BEEN EXECUTED
'
'
   SOUND 1000, .5
   SOUND 2000, .5
   SOUND 3000, .5
'
END SUB

SUB BEEP2 STATIC
' THIS PROCEDURE ENABLES THE COMPUTER TO AUDIBLY SIGNAL THE USER WHEN
' THE FINAL RESULTS ARE ABOUT TO BE PRINTED ON THE SCREEN *)
'
'
   SOUND 3000, .25
   SOUND 2000, .25
   SOUND 3000, .25
   SOUND 4000, .25
'
END SUB

FUNCTION CALCRANGE (energy, material%) STATIC
'
' THIS FUNCTION DOES A LINEAR INTERPOLATION TO DETERMINE THE RANGE OF THE
' ALPHA PARTICLE BASED ON THE VALUES IN THE RANGE TABLE.
'
   j = 0
   DO
      j = j + 1
      fraction = (RangeTable(0, j) - energy) / (RangeTable(0, j) - RangeTable(0, j - 1))
   LOOP UNTIL fraction >= 0
   CALCRANGE = RangeTable(material%, j) - fraction * (RangeTable(material%, j) -
RangeTable(material%, j - 1))
'
END FUNCTION

SUB CHANGEVAR STATIC
'
' THIS SUBROUTINE ALLOWS THE USER TO MAKE CHANGES TO THE VARIABLES
'
   SHARED energy, radius, AePore, density, events%, minenergy
   SHARED AeSphere, densitysphere, porosity
   PRINT
   PRINT
   CALL VARLIST
   INPUT "ENTER CODE FOR THE FIRST MODIFICATION  "; code
   DO
      IF (code <> 0) THEN
         SELECT CASE code
            CASE 1
```

```
            INPUT "ENTER NEW VALUE FOR ENERGY  "; energy
         CASE 2
            INPUT "ENTER NEW VALUE FOR RADIUS  "; radius
         CASE 3
            INPUT "ENTER NEW VALUE FOR EFFECTIVE ATOMIC MASS  "; AePore
         CASE 4
            INPUT "ENTER NEW VALUE FOR DENSITY  "; density
         CASE 5
            INPUT "ENTER NEW EFFECTIVE ATOMIC MASS FOR THE SOLID  "; AeSphere
         CASE 6
            INPUT "ENTER NEW SOLID DENSITY  "; densitysphere
         CASE 7
            INPUT "ENTER NEW VALUE FOR NUMBER OF EVENTS  "; events%
         CASE 8
            INPUT "ENTER NEW VALUE FOR MINIMUM ENERGY  "; minenergy
         CASE 9
            INPUT "ENTER NEW POROSITY ( > 0.26)"; porosity
         CASE ELSE
            PRINT "NOT AN APPROPRIATE CODE. TRY AGAIN!')"
      END SELECT
      INPUT "ENTER CODE FOR NEXT MODIFICATION  "; code
   END IF
LOOP UNTIL code = 0
PRINT
END SUB

SUB COMBINEDATA (k) STATIC
'This subroutine combines the data into the output file.
'
SHARED events%, OutputFile$
EnergyOut$ = OutputFile$ + ".PRN"
OPEN EnergyOut$ FOR OUTPUT AS #(k + 2)
FOR j = 0 TO k
   IF j < 10 THEN
      TemporaryFile$ = "EDEP" + RIGHT$(STR$(j), 1) + ".dat"
      ELSE
         TemporaryFile$ = "EDEP" + RIGHT$(STR$(j), 2) + ".dat"
   END IF
   OPEN TemporaryFile$ FOR INPUT AS #(j + 1)
NEXT j
FOR i = 1 TO events%
   FOR j = 1 TO k + 1
      INPUT #j, transfer
      PRINT #(k + 2), USING "####.####"; transfer;
      PRINT #(k + 2), ",";
   NEXT j
   PRINT #(k + 2),
NEXT i
CLOSE
FOR j = 0 TO k
   IF j < 10 THEN
      TemporaryFile$ = "EDEP" + RIGHT$(STR$(j), 1) + ".dat"
```

```
        ELSE
            TemporaryFile$ = "EDEP" + RIGHT$(STR$(j), 2) + ".dat"
        END IF
        KILL TemporaryFile$
    NEXT j
PRINT "YOUR INPUT PARAMETERS FOR THIS RUN ARE STORED IN FILE "; OutputFile$; ".INF"
PRINT "YOUR RADIUS AND EFFICIENCY DATA ARE STORED IN FILE "; OutputFile$; "R.PRN"
PRINT "THE ENERGIES DEPOSITED IN SPHERES FOR EACH EVENT ARE IN "; EnergyOut$

END SUB

SUB EDEP (pcntrangeto1, pcntrangeto2, edepinsphere, WHICHSPHERE%) STATIC
    'This subroutine calculates the energy deposited in a sphere if the
    'alpha completely transits the sphere.
    '
    SHARED density, densitysphere, AePore, AeSphere, energy, range
    SHARED XI, YI, ZI, X1, Y1, Z1, X2, Y2, Z2, VX, VY, VZ, XF, YF, ZF, i
    '
    'Calculate residual range in liquid:
    '
    IF pcntrangeto1 < pcntrangeto2 THEN
        residualrange = range * (1 - pcntrangeto1)
        ELSE
            residualrange = range * (1 - pcntrangeto2)
    END IF
    '
    'Calculate energy remaining to alpha particle:
    '
    resenergysolid = EnergyLeft(2, residualrange)
    '
    rangesolid = CALCRANGE(resenergysolid, 1)
    distancethroughsphere = ABS(pcntrangeto1 - pcntrangeto2) * range
    IF rangesolid <= distancethroughsphere THEN
        'The alpha doesn't make it through, so sub ENERGYDEPOSITION can be used.
        CALL ENERGYDEPOSITION(residualrange, edepinsphere)
        ELSE
            resrangesolid = rangesolid - distancethroughsphere
            resenergyliquid = EnergyLeft(1, resrangesolid)
            edepinsphere = edepinsphere + resenergysolid - resenergyliquid
            range = CALCRANGE(resenergyliquid, 2)
            IF pcntrangeto1 > pcntrangeto2 THEN
                XI = X1
                YI = Y1
                ZI = Z1
                ELSE
                    XI = X2
                    YI = Y2
                    ZI = Z2
            END IF
            CALL NORMVECTOR(VX, VY, VZ, range)
            IF (XI ^ 2 >= L ^ 2) OR (YI ^ 2 >= L ^ 2) OR (ZI ^ 2 >= L ^ 2) THEN
                CALL MOVETONEXTCUBE(XI, YI, ZI)
```

```
            END IF
            CALL ADDVECTOR
        END IF
    END SUB

    SUB ENERGYDEPOSITION (residualrange, edepinsphere) STATIC
        'This subroutine calculates the energy deposited in a sphere
        'if the alpha doesn't make it through the sphere.
        '
        SHARED density, AePore, i
        '
        i = 6 ' Exit DO loop in sub WHEREISIT
        edepinsphere = edepinsphere + EnergyLeft(2, residualrange)
    END SUB

    SUB EnergyInterp STATIC
        'This subroutine creates range - energy tables for the two materials.
        'It uses an equation developed by H. H. Ross to calculate the alpha range
        'in air.  The alpha range in the material of interest is calculated using
        'equation 4-8 from "Nuclear and Radiochemistry", 2nd Edition,
        'G. Friedlander, J. Kennedy, and J. Miller, 1964.
        '
        SHARED AePore, AeSphere, density, densitysphere
        RangeTable(0, 0) = 0
        RangeTable(1, 0) = 0
        RangeTable(2, 0) = 0
        FOR j = 1 TO 20
            'Energy in MeV:
            RangeTable(0, j) = j / 2
            rangeair = .377 * (j / 2) ^ 1.39
            IF AeSphere <= 20 THEN
                factor1 = 1 + (.02606 - (.001867 * AeSphere)) * LOG(j / 8)
                ELSE
                    factor1 = (.9 + .01375 * AeSphere) + (.02606 - (.001867 * AeSphere)) * LOG(j / 8)
            END IF
            IF AePore <= 20 THEN
                factor2 = 1 + (.02606 - (.001867 * AePore)) * LOG(j / 8)
                ELSE
                    factor2 = (1 + .01375 * AePore) + (.02606 - (.001867 * AePore)) * LOG(j / 8)
            END IF
            'Range in sphere material:
            RangeTable(1, j) = (rangeair * factor1 - .0025 * AeSphere) / (densitysphere * 1000)
            'Range in pore material:
            RangeTable(2, j) = (rangeair * factor2 - .0025 * AePore) / (density * 1000)
        NEXT j
    END SUB

    FUNCTION EnergyLeft (material%, residualrange) STATIC
        'This function does a linear interpolation to find the energy remaining
        'to the alpha particle based on its residual range.
        j = 0
        DO
```

```
        j = j + 1
        fraction = (RangeTable(material%, j) - residualrange) / (RangeTable(material%, j) -
RangeTable(material%, j - 1))
    LOOP UNTIL fraction >= 0
    NewEnergy = RangeTable(0, j) - fraction * (RangeTable(0, j) - RangeTable(0, j - 1))
    IF NewEnergy < 0 THEN
        NewEnergy = 0
    END IF
    EnergyLeft = NewEnergy
END FUNCTION

SUB EXITCUBEPOINT (XI, YI, ZI, range) STATIC
    'This subroutine finds the point where the alpha exits the unit cube,
    'if it doesn't exit the cube through a point within a sphere.
    '
    DIM time(2, 6)
    SHARED L, VX, VY, VZ, LONGRANGEFLAG%, XF, YF, ZF
    FOR j = 1 TO 6
        time(1, j) = j
    NEXT j
    IF VX ^ 2 < 1E-20 THEN
        time(2, 1) = -1
        time(2, 2) = -1
        ELSE
            time(2, 1) = (L - XI) / VX
            time(2, 2) = -(L + XI) / VX
    END IF
    IF VY ^ 2 < 1E-20 THEN
        time(2, 3) = -1
        time(2, 4) = -1
        ELSE
            time(2, 3) = (L - YI) / VY
            time(2, 4) = -(L + YI) / VY
    END IF
    IF VZ ^ 2 < 1E-20 THEN
        time(2, 5) = -1
        time(2, 6) = -1
        ELSE
            time(2, 5) = (L - ZI) / VZ
            time(2, 6) = -(L + ZI) / VZ
    END IF
    FOR k = 5 TO 1 STEP -1
        FOR j = 1 TO k
            IF time(2, j) > time(2, j + 1) THEN
                SWAP time(1, j), time(1, j + 1)
                SWAP time(2, j), time(2, j + 1)
            END IF
        NEXT j
    NEXT k
    j = 0
    DO
        j = j + 1
```

```
        timetoside = time(2, j)
    LOOP UNTIL timetoside > 0 OR (timetoside = 0 AND j > 3)
    exitside = time(1, j)
    distancetoside = timetoside * SQR(VX ^ 2 + VY ^ 2 + VZ ^ 2)
    IF distancetoside < range THEN
        'Move initial point to point where alpha exits the cube:
        XI = XI + VX * timetoside
        YI = YI + VY * timetoside
        ZI = ZI + VZ * timetoside
        range = range - distancetoside
        CALL NORMVECTOR(VX, VY, VZ, range)
        LONGRANGEFLAG% = -1
        'Translate initial point so that alpha enters cube:
        SELECT CASE exitside
            CASE 1
                XI = XI - 2 * L
            CASE 2
                XI = XI + 2 * L
            CASE 3
                YI = YI - 2 * L
            CASE 4
                YI = YI + 2 * L
            CASE 5
                ZI = ZI - 2 * L
            CASE 6
                ZI = ZI + 2 * L
        END SELECT
        CALL ADDVECTOR
    END IF
END SUB

FUNCTION FITSPHERES (X, Y, Z) STATIC
'
' THIS FUNCTION DETERMINES WHETHER A POINT IS WITHIN ONE OF THE FOURTEEN
' FCC SPHERES.
'
    SHARED radius, L
    FITSPHERES = 0
    FOR i = 0 TO 1
        Const1 = (X - L * (-1) ^ i) ^ 2
        Const2 = (Y - L * (-1) ^ i) ^ 2
        Const3 = (Z - L * (-1) ^ i) ^ 2
        IF ((Const1 + Y ^ 2 + Z ^ 2) <= radius ^ 2) THEN
            FITSPHERES = -1
            ELSEIF ((X ^ 2 + Const2 + Z ^ 2) <= radius ^ 2) THEN
                FITSPHERES = -1
            ELSEIF ((X ^ 2 + Y ^ 2 + Const3) <= radius ^ 2) THEN
                FITSPHERES = -1
            ELSEIF ((Const1 + Const2 + Const3) <= radius ^ 2) THEN
                FITSPHERES = -1
            ELSEIF (((X + L * (-1) ^ i) ^ 2 + Const2 + Const3) <= radius ^ 2) THEN
                FITSPHERES = -1
```

```
        ELSEIF ((Const1 + (Y + L * (-1) ^ i) ^ 2 + Const3) <= radius ^ 2) THEN
            FITSPHERES = -1
        ELSEIF ((Const1 + Const2 + (Z + L * (-1) ^ i) ^ 2) <= radius ^ 2) THEN
            FITSPHERES = -1
      END IF
   NEXT i
END FUNCTION

SUB HELLO STATIC
'THIS PROCEDURE WRITES AS SHORT INTRODUCTION TO THE PROGRAM ON THE SCREEN
   CLS
   PRINT ;
   PRINT ;
   PRINT ;
   PRINT ;
   PRINT "**************************************************"
   PRINT "*                                                *"
   PRINT "*  HELLO!                                        *"
   PRINT "*                                                *"
   PRINT "*  THIS PROGRAM WAS MODIFIED BY M. E. KEILLOR    *"
   PRINT "*  FROM A PROGRAM WRITTEN BY H. H. ROSS          *"
   PRINT "*  AND L. L. ROZEVINK. THE PROGRAM ASSUMES A     *"
   PRINT "*  FACE CENTERED CUBIC UNIT CELL AND A STRAIGHT  *"
   PRINT "*  LINE ALPHA TRACK.  EACH ALPHA IS FOLLOWED TO  *"
   PRINT "*  THE END OF ITS TRACK, WITH THE ENERGY         *"
   PRINT "*  DEPOSITED IN SPHERES CALCULATED USING A       *"
   PRINT "*  RESIDUAL RANGE METHOD.                        *"
   PRINT "**************************************************"
   PRINT ;
   PRINT ;
   INPUT "PRESS RETURN WHEN READY TO PROCEED"; DUMMY
END SUB

SUB INITVAR STATIC
'
' THIS PROCEDURE INITIALIZES SEVERAL VARIABLES
'
   SHARED L, radius, MasterCounter%, DISCRIMINATOR, minenergy
   SHARED energy, porosity, pi, InVoidVol
   SHARED InCubeInSphere, LongRangeDetLight%, NotCubeInSphere%, PcntInCube
   SHARED OutLeavesEnergy%, InLeavesEnergy, LongRangeCount%, DetAsLightCount%
   InCubeInSphere = 0
   LongRangeDetLight% = 0
   NotCubeInSphere% = 0
   PcntInCube = 0
   InVoidVol = 0
   OutLeavesEnergy% = 0
   InLeavesEnergy = 0
   LongRangeCount% = 0
   DetAsLightCount% = 0
   MasterCounter% = 0
   DISCRIMINATOR = minenergy * .001 / energy
```

```
    'Coordinate for sphere centers:
    L = radius * (2 * pi / (3 * (1 - porosity))) ^ (1 / 3)
    CENTERS(1, 1) = L
    CENTERS(2, 1) = -L
    CENTERS(3, 2) = L
    CENTERS(4, 2) = -L
    CENTERS(5, 3) = L
    CENTERS(6, 3) = -L
    FOR j = 1 TO 3
        CENTERS(7, j) = L
        CENTERS(8, j) = -L
        CENTERS(9, j) = L
        CENTERS(10, j) = L
        CENTERS(11, j) = L
        CENTERS(12, j) = -L
        CENTERS(13, j) = -L
        CENTERS(14, j) = -L
    NEXT j
    CENTERS(9, 3) = -L
    CENTERS(10, 1) = -L
    CENTERS(11, 2) = -L
    CENTERS(12, 1) = L
    CENTERS(13, 2) = L
    CENTERS(14, 3) = L
END SUB

SUB INTERSECTIONS (XI, YI, ZI, A, B, C, D, E, F) STATIC
'
' AN INFINITE LINE HAS JUST BEEN DRAWN THROUGH THE VECTOR...
' THIS PROCEDURE CALCULATES HOW MANY TIMES THE LINE INTERSECTS
' A SPHERE WITH ITS CENTER AT (D, E, F)
'
    SHARED range, VZ, VX, VY, INTERCEPTS, radius
    A = range ^ 2
    B = 2 * ((XI - D) * VX + (YI - E) * VY + (ZI - F) * VZ)
    C = (XI - D) ^ 2 + (YI - E) ^ 2 + (ZI - F) ^ 2 - radius ^ 2
'
    IF (B ^ 2 - (4 * A * C)) >= 0 THEN
        IF (B ^ 2 - (4 * A * C) = 0) THEN
            INTERCEPTS = 1
            ELSE INTERCEPTS = 2
        END IF
        ELSE INTERCEPTS = 0
    END IF
END SUB

SUB MOVETONEXTCUBE (XI, YI, ZI) STATIC
    'This subroutine translates the particle initial point so that the alpha
    'particle continues to traverse the unit cell.
    '
    SHARED L, LONGRANGEFLAG%
    '
```

```
    LONGRANGEFLAG% = -1
    IF (XI >= L) THEN
       XI = XI - 2 * L
       ELSEIF (XI <= -L) THEN
          XI = XI + 2 * L
    END IF
    IF (YI >= L) THEN
       YI = YI - 2 * L
       ELSEIF (YI <= -L) THEN
          YI = YI + 2 * L
    END IF
    IF (ZI >= L) THEN
       ZI = ZI - 2 * L
       ELSEIF (ZI <= -L) THEN
          ZI = ZI + 2 * L
    END IF
END SUB

SUB NORMVECTOR (VX, VY, VZ, length) STATIC
'
' THIS PROCEDURE SHRINKS/LENGTHENS THE VECTOR SO THAT THE NORM OF THE
' NEW VECTOR EQUALS THE VALUE PASSED TO THE VARIABLE "length"
'
    norm = SQR(VX ^ 2 + VY ^ 2 + VZ ^ 2)
    VX = VX / norm * length
    VY = VY / norm * length
    VZ = VZ / norm * length
END SUB

SUB PICKCOORD STATIC
' THIS PROCEDURE RANDOMLY CHOOSES VALUES FOR THE INITIAL COORDINATES
' OF THE ALPHA-PARTICLE, WITHIN THE PORE VOLUME BETWEEN SPHERES PACKED
' IN A FACE CENTERED CUBIC ARRANGEMENT.
'
    SHARED MasterCounter%, XI, YI, ZI, radius, L
    DO
       MasterCounter% = MasterCounter% + 1
       ZI = (2 * RND - 1) * L
       XI = (2 * RND - 1) * L
       YI = (2 * RND - 1) * L
    LOOP UNTIL NOT FITSPHERES(XI, YI, ZI)
END SUB

SUB PICKCOORDADSORBED STATIC
' THIS PROCEDURE RANDOMLY CHOOSES VALUES FOR THE INITIAL COORDINATES
' OF THE ALPHA-PARTICLE, ON THE SURFACE OF ONE OF THE FOURTEEN SPHERES
' (AND WITHIN THE UNIT CELL)...
' THE CENTER OF THE COORDINATE SYSTEM IS THE CENTER OF A FACE CENTERED
' CUBIC UNIT CELL
'
    SHARED MasterCounter%, radius, XI, YI, ZI, L
    DO
```

```
        MasterCounter% = MasterCounter% + 1
        WHICHSPHERE% = FIX(RND * 14) + 1
        xvector = (RND * 2) - 1
        yvector = (RND * 2) - 1
        zvector = (RND * 2) - 1
        CALL NORMVECTOR(xvector, yvector, zvector, radius)
        D = CENTERS(WHICHSPHERE%, 1)
        E = CENTERS(WHICHSPHERE%, 2)
        F = CENTERS(WHICHSPHERE%, 3)
        XI = D + xvector
        YI = E + yvector
        ZI = F + zvector
        GOODIP = (XI ^ 2 < L ^ 2 AND YI ^ 2 < L ^ 2 AND ZI ^ 2 < L ^ 2)
    LOOP UNTIL GOODIP
END SUB

SUB PICKVECTOR STATIC
'
' THIS PROCEDURE RANDOMLY SELECTS VECTOR COMPONENTS
'
    SHARED VX, VY, VZ
    VX = (RND * 2) - 1
    VY = (RND * 2) - 1
    VZ = (RND * 2) - 1

END SUB

SUB SPHERE (WHICHSPHERE%, D, E, F, edepinsphere) STATIC
'
' THIS SUBROUTINE DETERMINES THE DISTANCE TO ALPHA INTERSECTIONS WITH A
' SPHERES SURFACE, AND CALLS THE APPROPRIATE ENERGY DEPOSITION ROUTINE.
'
    SHARED INTERCEPTS, A, B, C, XI, YI, ZI, XF, YF, ZF, VX, VY, VZ, range
    SHARED X1, X2, Y1, Y2, Z1, Z2, pcntrangeto1(), pcntrangeto2(), i
    IF i > 1 THEN
        CALL INTERSECTIONS(XI, YI, ZI, A, B, C, D, E, F)
        pcntrangeto1(WHICHSPHERE%) = (-B + SQR(B ^ 2 - (4 * A * C))) / (2 * A)
        pcntrangeto2(WHICHSPHERE%) = (-B - SQR(B ^ 2 - (4 * A * C))) / (2 * A)
    END IF
    Z1 = ZI + pcntrangeto1(WHICHSPHERE%) * VZ
    Z2 = ZI + pcntrangeto2(WHICHSPHERE%) * VZ
    X1 = XI + pcntrangeto1(WHICHSPHERE%) * VX
    X2 = XI + pcntrangeto2(WHICHSPHERE%) * VX
    Y1 = YI + pcntrangeto1(WHICHSPHERE%) * VY
    Y2 = YI + pcntrangeto2(WHICHSPHERE%) * VY
    criteria1 = pcntrangeto1(WHICHSPHERE%) > -.000001
    criteria2 = pcntrangeto2(WHICHSPHERE%) > -.000001
    criteria3 = pcntrangeto1(WHICHSPHERE%) <= 1
    criteria4 = pcntrangeto2(WHICHSPHERE%) <= 1
    IF criteria1 AND criteria2 THEN
        IF criteria3 AND criteria4 THEN
```

```
        CALL EDEP(pcntrangeto1(WHICHSPHERE%), pcntrangeto2(WHICHSPHERE%),
edepinsphere, WHICHSPHERE%)
        '
        ELSEIF criteria3 THEN
            residualrange = (1 - pcntrangeto1(WHICHSPHERE%)) * range
            CALL ENERGYDEPOSITION(residualrange, edepinsphere)
        ELSEIF criteria4 THEN
            residualrange = (1 - pcntrangeto2(WHICHSPHERE%)) * range
            CALL ENERGYDEPOSITION(residualrange, edepinsphere)
      END IF
   END IF
END SUB

SUB SPHERESEQUENCE STATIC
   'This subroutine determines the sequence of spheres along the path
   'of the alpha particle.
   '
   SHARED INTERCEPTS, A, B, C, XI, YI, ZI, XF, YF, ZF, VX, VY, VZ, range
   SHARED X1, X2, Y1, Y2, Z1, Z2, pcntrangeto1(), pcntrangeto2(), SEQUENCE%()
   SHARED radius
   index = 1
   FOR i = 1 TO 5
      SEQUENCE%(i) = 0
   NEXT i
   FOR WHICHSPHERE% = 1 TO 14
      pcntrangeto1(WHICHSPHERE%) = 0
      pcntrangeto2(WHICHSPHERE%) = 0
      D = CENTERS(WHICHSPHERE%, 1)
      E = CENTERS(WHICHSPHERE%, 2)
      F = CENTERS(WHICHSPHERE%, 3)
      CALL INTERSECTIONS(XI, YI, ZI, A, B, C, D, E, F)
      IF INTERCEPTS = 2 THEN
         pcntrangeto1(WHICHSPHERE%) = (-B + SQR(B ^ 2 - (4 * A * C))) / (2 * A)
         pcntrangeto2(WHICHSPHERE%) = (-B - SQR(B ^ 2 - (4 * A * C))) / (2 * A)
         criteria1 = pcntrangeto1(WHICHSPHERE%) > 0
         criteria2 = pcntrangeto2(WHICHSPHERE%) > -(radius / 1000)
         IF criteria1 AND criteria2 THEN
            SEQUENCE%(index) = WHICHSPHERE%
            index = index + 1
         END IF
      END IF
   NEXT WHICHSPHERE%
   '
   IF index > 2 THEN
      FOR k = (index - 2) TO 1 STEP -1
         FOR j = 1 TO k
            IF pcntrangeto1(SEQUENCE%(j)) > pcntrangeto1(SEQUENCE%(j + 1)) THEN
               SWAP SEQUENCE%(j), SEQUENCE%(j + 1)
            END IF
         NEXT j
      NEXT k
   END IF
```

```
'
END SUB

SUB USERINPUT STATIC
' THIS SUBROUTINE ALLOWS THE USER TO ENTER THE FIRST SET OF VARIABLES.
' IT ALSO STARTS WRITING THE OUTPUT FILE.
'
   SHARED energy, radius, AePore, AeSphere, density, minenergy, events%
   SHARED maxradius, stepsize, densitysphere, porosity, pi, OutputFile$
   SHARED AdsorbedFlag%, steps%, version$
   INPUT "ENTER ENERGY OF ALPHA PARTICLE IN MEV:"; energy
   'INPUT "ENTER RADIUS OF SPHERES IN CM:  "; radius
   INPUT "Enter Minimum Radius of interest (cm):  "; radius
   INPUT "Enter step size for incrementing radius (cm):  "; stepsize
   INPUT "ENTER NUMBER OF TIMES TO INCREMENT RADIUS (0 to 10):  "; steps%
   'INPUT "Enter Maximimum radius of interest:  "; maxradius
   PRINT
   PRINT "THE EFFECTIVE ATOMIC MASS IS GIVEN BY THE FOLLOWING:"
   PRINT
   PRINT "                                    [aA + bB + cC + ...]^2"
   PRINT "   Effective Atomic Mass = ----------------------------------"
   PRINT "                           [a(A)^.5 + b(B)^.5 + c(C)^.5 + ...]^2"
   PRINT
   '
   PRINT "WHERE THE SMALL LETTERS REPRESENT THE NUMBER OF ATOMS OF THE
ELEMENTS";
   PRINT "AND THE LARGE LETTERS REPRESENT THE ATOMIC MASS OF THE ELEMENTS"
   PRINT
   INPUT "ENTER EFFECTIVE ATOMIC MASS OF LIQUID"; AePore
   INPUT "ENTER EFFECTIVE ATOMIC MASS OF SOLID"; AeSphere
   INPUT "ENTER DENSITY OF LIQUID IN G/CM^3"; density
   INPUT "ENTER DENSITY OF SOLID IN G/CM^3"; densitysphere
   INPUT "ENTER DESIRED POROSITY ( >= 0.26)(PRESS ENTER FOR DEFAULT)"; porosity
   IF porosity = 0 THEN
      porosity = 1 - pi / (3 * SQR(2))
   END IF
   DO
      loopflag% = -1
      INPUT "EMITTERS ADSORBED (A) OR DISTRIBUTED THROUGH PORE (D)?"; answer$
      SELECT CASE answer$
         CASE "A", "a"
            AdsorbedFlag% = -1
         CASE "D", "d"
            AdsorbedFlag% = 0
         CASE ELSE
            PRINT "That isn't a valid input. Please try again."
            loopflag% = 0
      END SELECT
   LOOP UNTIL loopflag%
   INPUT "ENTER NUMBER OF EVENTS"; events%
   'INPUT "ENTER MINIMUM ENERGY IN KEV NEEDED TO PRODUCE LIGHT"; minenergy
   minenergy = 0
```

```
    INPUT "ENTER FILE NAME FOR OUTPUT(7 CHAR MAX, NO EXTENSION)"; OutputFile$
    PRINT ;
    '
    'Print input parameters into output file:
    InfoFile$ = OutputFile$ + ".inf"
    OPEN InfoFile$ FOR OUTPUT AS #1
    PRINT #1, "Monte Carlo Experiment Run Using Program "; version$
    PRINT #1, "Date: "; DATE$
    PRINT #1, "Time: "; TIME$
    PRINT #1,
    PRINT #1, "Input Parameters:"
    PRINT #1,
    PRINT #1, "Energy of Alpha Particle: "; energy; "  MeV"
    PRINT #1, "Effective Atomic Mass of Spheres: "; AeSphere
    PRINT #1, "Effective Atomic Mass of Pores: "; AePore
    PRINT #1, "Sphere Density: "; densitysphere; "  g/cm^3"
    PRINT #1, "Pore Density: "; density; "  g/cm^3"
    PRINT #1, "Porosity: "; porosity * 100; " %"
    IF AdsorbedFlag% THEN
       PRINT #1, "Alpha emitters adsorbed on surface of spheres."
       ELSE
          PRINT #1, "Alpha emitters distributed through volume of pore."
    END IF
    PRINT #1,
    PRINT #1, "The sphere radius (in microns) and detection efficiency data"
    PRINT #1, "are stored in file "; OutputFile$; "R.PRN"
    PRINT #1, "The energies deposited in spheres for each event are stored"
    PRINT #1, "in file "; OutputFile$; ".prn"
    CLOSE #1
    Eff$ = OutputFile$ + "R.PRN"
    OPEN Eff$ FOR OUTPUT AS #1
END SUB

SUB VARLIST STATIC
'
' THIS PROCEDURE PRINTS A TABLE OF VALUES FOR THE VARIABLES THE USER
' HAS INITIALIZED AND ALLOWS CHANGES.
'
    SHARED energy, radius, AePore, density, events%, minenergy
    SHARED AeSphere, densitysphere, porosity
    PRINT "************************************************"
    PRINT "*"
    PRINT "*  CODE   DESCRIPTION      VALUE"
    PRINT "*_____________________________________________"
    PRINT "*"
    PRINT "*   1     ENERGY          "; energy
    PRINT "*   2     MIN RADIUS       "; radius
    PRINT "*  "
    PRINT "*         LIQUID:"
    PRINT "*   3     EFF AT MASS      "; AePore
    PRINT "*   4     DENSITY         "; density
    PRINT "*"
```

```
    PRINT "*         SOLID:"
    PRINT "*   5     EFF ATOMIC MASS    "; AeSphere
    PRINT "*   6     DENSITY            "; densitysphere
    PRINT "*"
    PRINT "*   7     # EVENTS           "; events%
    PRINT "*   8     MIN ENERGY         "; minenergy
    PRINT "*   9     POROSITY           "; porosity
    PRINT "*"
    PRINT "*   0     NO CHANGES"
    PRINT "*"
    PRINT "************************************************"
    PRINT
    PRINT
END SUB

SUB VARSUMMARY STATIC
' THIS SUBROUTINE PRINTS A SUMMARY OF INPUT PARAMETER VALUES
'
    SHARED energy, radius, AePore, density, events%, minenergy, range
    SHARED AeSphere, densitysphere, porosity
    SHARED RangeSave
    PRINT "************************************************"
    PRINT "*"
    PRINT "*  CODE    DESCRIPTION       VALUE"
    PRINT "* ____________________________________________"
    PRINT "*"
    PRINT "*   1     ENERGY             "; energy
    PRINT "*   2     RADIUS             "; radius
    PRINT "*"
    PRINT "          LIQUID:"
    PRINT "*   3     EFF ATOMIC MASS    "; AePore
    PRINT "*   4     DENSITY            "; density
    PRINT "*"
    PRINT "*         SOLID:"
    PRINT "*   5     EFF ATOMIC MASS    "; AeSphere
    PRINT "*   6     DENSITY            "; densitysphere
    PRINT "*"
    PRINT "*   7     # EVENTS           "; events%
    PRINT "*   8     MIN ENERGY         "; minenergy
    PRINT "*   9     POROSITY           "; porosity
    PRINT "*"
    PRINT "*         RANGE IN LIQUID    "; RangeSave
    PRINT "*"
    PRINT "************************************************"
    PRINT
    PRINT
END SUB

SUB WHEREISIT (XF, YF, ZF, InLeavesEnergy, OutLeavesEnergy%) STATIC
'
' THIS PROCEDURE FINDS WHERE THE FINAL POINT IS: INSIDE THE VOID VOLUME,
' IN ONE OF THE FOURTEEN SPHERES, OR BEYOND THE FOURTEEN SPHERES
```

```
'
SHARED L, InCubeInSphere, DISCRIMINATOR, SEQUENCE%(), i
SHARED InVoidVol, NotCubeInSphere%, LONGRANGEFLAG%
SHARED LongRangeDetLight%, LongRangeCount%, edepinsphere, XI, YI, ZI, range
'
criteria1 = XF ^ 2 < L ^ 2
criteria2 = YF ^ 2 < L ^ 2
criteria3 = ZF ^ 2 < L ^ 2
criteria4 = FITSPHERES(XF, YF, ZF)
edepinsphere = 0
CALL SPHERESEQUENCE
i = 1
DO
   IF SEQUENCE%(i) = 0 THEN
      'Check if alpha leaves cube through void space
       CALL EXITCUBEPOINT(XI, YI, ZI, range)
      IF LONGRANGEFLAG% THEN
         CALL SPHERESEQUENCE
         LONGRANGEFLAG% = 0
         i = 1
         ELSE
            i = 6
      END IF
      ELSE
         D = CENTERS(SEQUENCE%(i), 1)
         E = CENTERS(SEQUENCE%(i), 2)
         F = CENTERS(SEQUENCE%(i), 3)
         CALL SPHERE(SEQUENCE%(i), D, E, F, edepinsphere)
         IF LONGRANGEFLAG% THEN
            CALL SPHERESEQUENCE
            LONGRANGEFLAG% = 0
            i = 1
            ELSE
               IF i < 6 THEN
                                                    i = i + 1
               END IF
         END IF
   END IF
'PRINT "edepinsphere = "; edepinsphere
LOOP UNTIL i = 6
PRINT #2, USING "####.####"; edepinsphere;
'
IF criteria1 AND criteria2 AND criteria3 THEN
   IF edepinsphere > (DISCRIMINATOR * 100) THEN
      InLeavesEnergy = InLeavesEnergy + 1
   END IF
   IF criteria4 THEN
      InCubeInSphere = InCubeInSphere + 1
      ELSE
         InVoidVol = InVoidVol + 1
   END IF
   ELSE
```

```
            IF criteria4 THEN
               NotCubeInSphere% = NotCubeInSphere% + 1
               IF edepinsphere > (DISCRIMINATOR * 100) THEN
                  OutLeavesEnergy% = OutLeavesEnergy% + 1
                  ELSE STOP
               END IF
               ELSE
                  LongRangeCount% = LongRangeCount% + 1
                  IF edepinsphere > (DISCRIMINATOR * 100) THEN
                     LongRangeDetLight% = LongRangeDetLight% + 1
                     OutLeavesEnergy% = OutLeavesEnergy% + 1
                  END IF
            END IF
      END IF
END SUB

SUB WRITTENSUMMARY (InLeavesEnergy, OutLeavesEnergy%) STATIC
'
' THIS PROCEDURE PRINTS A SUMMARY OF DETECTION EFFICIENCY INFORMATION.
' IT ALSO STORES RADIUS AND EFFICIENCY DATA TO THE OUTPUT FILE.
'
   SHARED radius, energy, minenergy, AePore, density, GoodPoints%
   SHARED InVoidVol, NotCubeInSphere%, InCubeInSphere, LongRangeCount%
   SHARED DetAsLightCount%, MasterCounter%
   SHARED LongRangeDetLight%
   DetAsLightCount% = InLeavesEnergy + OutLeavesEnergy%
   detefficiency = DetAsLightCount% / GoodPoints%
   PRINT
   PRINT "*************************************************************"
   PRINT "*"
   PRINT "*  Radius = "; radius; "  cm"
   PRINT "*  Alpha Energy = "; energy; "  MeV"
   PRINT "*  Minimum Energy = "; minenergy; "keV"
   PRINT "*  Effective Atomic Mass = "; AePore; " g/mole"
   PRINT "*  Density = "; density; " g/cm^3"
   PRINT "*  # Events =  "; GoodPoints%
   PRINT "*"
   PRINT "*  In Cube -- In Void ======> "; InVoidVol; " Alphas"
   PRINT "*         -- In Spheres ==> "; InCubeInSphere; " Alphas"
   PRINT "*"
   PRINT "*  Not in Cube -- In Spheres ==>"; NotCubeInSphere%; " Alphas"
   PRINT "*           -- Beyond Spheres ==> "; LongRangeCount%; " Alphas"
   PRINT "*"
   PRINT "*  Alphas Generating Light in 1 of 5 Spheres ==>"; DetAsLightCount%; " Alphas"
   PRINT "*"
'
   IF minenergy <> 0 THEN
      PRINT "*  The Detection Efficiency is "; detefficiency * 100; " %"
      ELSE
         PRINT "*  The Geometric Efficiency is "; detefficiency * 100; " %"
   END IF
   PRINT "*"
```

```
PRINT "*  TOTAL INITIAL POINTS GENERATED ==> ", MasterCounter%
PRINT "*"
PRINT "************************************************************"
PRINT #1, USING "####.####"; radius * 10000;
PRINT #1, ",";
PRINT #1, USING "####.####"; detefficiency
END SUB
```

Appendix B: Preparation of Polonium Source Solutions

Polonium can be extracted from weakly acidic solutions via spontaneous deposition on silver (Figgins, 29: 1961). This characteristic was exploited to remove ^{210}Po from an RaDEF solution onto a silver needle. The polonium was then removed from the silver by three different procedures, which will be presented below.

Polonium Extraction

1. A silver needle was stood on end in 2 ml of 0.5 N HCl containing roughly 8.5 μCi RaDEF (local identification #247). The silver was left in the solution for 1.5 hours.

2. After removal from the RaDEF solution, the needle was rinsed with 100 μl of 0.5 N HCl and again with 100 μl of 1.0 N HCl in an attempt to reduce ^{210}Pb and ^{210}Bi contamination. The rinse solution was allowed to fall back into the original RaDEF solution.

3. Polonium was removed from this silver sample for the three polonium source solutions discussed in Chapter 4. The silver was not reimmersed in the RaDEF source between preparation of the source solutions covered below.

Source Solution Procedures

Solution 247b.

1. 100 μl of NaOH solution (unknown concentration) was micropipetted over the silver and allowed to fall into a plastic vial. This procedure was accomplished with a heat lamp shining directly onto the silver.

2. 1 ml of deionized water was added to the vial using a 5 ml graduated cylinder.

3. The source was labelled #247b.

4. The solution was subsequently diluted by the addition of 2 ml of deionized water.

Solution 247c.

1. 250 μl of 12 N HCl was micropipetted over the silver and allowed to fall into a plastic vial containing 2.75 ml of deionized water.

2. The source was labelled #247c.

Solution 247c'.

1. Source solution 247c' was made up in the vial which still contained approximately 1.8 ml of solution 247c.

2. 2.75 ml deionized H_2O was added to the solution.

3. 250 μl of 12 N Nitric acid was pipetted over the silver needle and allowed to fall into the vial.

4. This solution retains the local identification #247c.

Appendix C: Mass Correction

A mass correction was applied to recorded masses for polonium solution added to gel-silica samples based on a systematic error in the mass values. The first iteration of data analysis yielded efficiencies on the order of 110% for detection of alpha particles in gel-silica. These results were significantly higher than the 100% expected, as well as difficult to explain on a physical basis. The data were reviewed and it was noted that masses for 10 μl drops of polonium source solution added to gel-silica samples were systematically lower than for those added to Ultima Gold in a counting vial. This error propagated into the efficiency calculations because the known specific activity was determined based on the mass of drops added to Ultima Gold, causing an underestimate for the amount of polonium added to gel-silica samples.

The error noted can be attributed to evaporation of the liquid during transport from the fume hood to the balance. All transfers of source solutions were performed under a fume hood for safety reasons. The balance used was 15 feet away from the hood, so that samples had to be carried from the hood to the balance after being doped. This transfer caused significantly more evaporation from the exposed surfaces of gel-silica samples than it did from drops added to scintillation cocktail in counting vials.

A correction factor for the mass of source solution added to gel-silica samples was determined experimentally. Table C-1 contains mass values for 10 ml drops of H_2O obtained using the same procedures as those used for the polonium source solutions. The

value of 6.43 mg in the second column was discarded based on Chauvenet's discard criteria of 2.24 σ for 20 measurements. The mean mass of drops added to a gel-silica sample was 9.15(0.08)mg, while it was 9.84(0.21)mg for drops added to Ultima Gold in a vial. This yields a correction factor of 1.075(0.025), which was used to arrive at the corrected masses reported in Table 4-4.

Table C-1. Data for Mass Correction

Drop	Mass Added to Ultima Gold (mg)	Mass Added to Gel-silica Sample (mg)
1	9.77	9.52
2	9.5	9.51
3	9.41	9.53
4	9.85	9.25
5	9.88	9.1
6	9.8	9.03
7	9.86	9.36
8	9.67	8.9
9	9.42	9.88
10	9.74	8.92
11	7.75	8.8
12	9.99	9.28
13	11.73	8.47
14	7.8	8.44
15	9.99	8.92
16	11.73	9.18
17	7.8	9.27
18	9.64	9.36
19	11.56	9.14
20	10.03	6.43

Bibliography

Bansal, N. P and Doremus, R. H. Handbook of Glass Properties. Orlando FL: Academic Press, Inc, 1986.

Birks, J. B. The Theory and Practice of Scintillation Counting. New York: The MacMillan Company, 1964.

Bevington, Philip R. and Robinson, D. K. Data Reduction and Error Analysis for the Physical Sciences, 2nd Ed. New York: McGraw-Hill, Inc., 1992.

Blanchard, Richard L. and others. "Radiological Sampling and Analytical Methods for National Primary Drinking Water Regulations," Health Physics, 48: 587-600 (1985).

Bouwer, Edward J., McKlveen, J. W. and McDowell, W. J. "A Solvent Extraction-Liquid Scintillation Method for Assay of Uranium and Thorium in Phosphate-Containing Material," Nuclear Technology, 42: 102-111 (January 1979).

Burggraf, L. W. Faculty, Air Force Institute of Technology. Personal Communication. Spring and Summer terms, 1994.

Case, G. N. and McDowell, W. J. "An Improved Sensitive Assay for Polonium-210 By Use of a Background-Rejecting Extractive Liquid-Scintillation Method," Talanta, 29: 845-848 (1982).

Cesini, G., Lucarini, G. and Rustichelli, F. "Evaluation of Fission Fragment Ranges in Any Medium," Nuclear Instruments and Methods, 127: 579-582 (1975).

Chiles, Marion M. "Evaluation of a Thin CaF_2(Eu) Scintillator for Detecting Tritium," IEEE Transactions on Nuclear Science, Vol NS-34, No 1: 386-388 (February 1981).

Davis, Richard M. Thesis Projects in Science and Engineering. New York: St. Martin's Press, 1980.

Everett, L. J. "Counting Performance and Resolution of an HPLC Radioactivity Monitor," Chromatographia, Vol 15, No 7: 445-448 (July 1982).

Figgins, P. E. The Radiochemistry of Polonium. Washington D. C.: The Office of Technical Services, Department of Commerce, 1961.

Friedlander, G., Kennedy, J. W. and Miller J. M. Nuclear and Radiochemistry, 2nd Ed. New York: John Wiley & Sons, Inc, 1964.

Harding, N. G. L. and others. "Low-Level Flow Counting of Liquid Chromatography Column Eluates," Chromatographia, Vol 15, No 7: 468-474 (July 1982).

Hench, L. L., Araujo, F. G., West, J. K, and La Torre, G. P. "Gel-Silica Optics: Theory and Application," in conference proceedings for the 7th International Workshop on Glasses & Ceramics from Gels,Paris, France, July 19-23, (1993).

Hench, L. L. and others. "Properties of Gel-silica Optical Matrices with 4.5 nm and 9.0 nm Pores," Proceedings of SPIE - The International Society for Optical Engineering: Volume 1758: Sol-Gel Optics II: 94-104 (1992)

Hench, L. L., Wang, S. H. and Nogues, J. L. "Gel-silica Optics," Proceedings of SPIE - The International Society for Optical Engineering: Volume 878: Multifunctional Materials: 76-85 (1988)

Hench, Larry L. and West, Jon K. Chemical Processing of Advanced Materials. New York: John Wiley & Sons, Inc. 1992.

Hench, L. L., West, J. K., Zhu, B. F. and Ochoa, R. "Gel-silica Hybrid Optics," Proceedings of SPIE - The International Society for Optical Engineering: Volume 1328: Sol-Gel Optics: 230-240 (1990)

Hofstetter, K. J. and Wilson, H. T. "Aqueous Effluent Tritium Monitor Development," Fusion Technology, 21: 446-451 (March 1992)

Horrocks, Donald L. and Studier, M. H. "Low Level Plutonium-241 Analysis by Liquid Scintillation Techniques," Analytical Chemistry, Vol 30, No 11: 1747-1750 (November 1958)

Iler, Ralph K. The Chemistry of Silica: Solubility, Polymerization, Colloid, and Surface Properties, and Biochemistry. New York: John Wiley & Sons, 1979.

Janni, J. F. "Proton Range-Energy Tables," Atomic Data and Nuclear Data Tables, Vol 27, Nos 2/3 (March, May 1982)

Kessler, Michael J. Liquid Scintillation Analysis: Science and Technology. Meriden, CT: Packard Instrument Company, 1989.

Knoll, Glenn F. Radiation Detection and Measurement. New York: John Wiley & Sons, 1989.

Knoll, Glenn F., Henderson, T. M. and Felmlee, W. J. "A Novel ^{3}He Scintillation Detector," IEEE Transactions on Nuclear Science, Vol NS-34, No 1: 473-474 (February 1981).
McCurdy, D. E. and Mellor, R. A. "The Concentration of 226Ra and 228Ra in Domestic and Imported Bottled Waters," Health Physics, 40: 250 (1981).

McDowell, W. J. "High-Resolution Liquid Scintillation Method for the Analytical Determination of Alpha-Emitters in Environmental Samples," IEEE Transactions on Nuclear Science, NS-22: 649-653 (February 1975)

McDowell, W. J. Alpha Counting and Spectrometry Using Liquid Scintillation Methods. Nuclear Science Series: Radiochemistry Techniques NAS-NS-3116 (DE86007601): January 1986.

McDowell, W. J., Farrar, D. T. and Billings, M. R. "Plutonium and Uranium Determination in Environmental Samples: Combined Solvent Extraction-Liquid Scintillation Method," Talanta, 21: 1231-1245 (1974)

McDowell, W. J. and McDowell, B. L. "Liquid Scintillation Alpha Spectrometry: A Method for Today and Tomorrow," in Liquid Scintillation Counting and Organic Scintillators. Ed. Harley Ross and others. Chelsea, MI: Lewis Publishers, 1991.

McKlveen, John W. and Johnson, W. R. "Simultaneous Alpha and Beta Particle Assay Using Liquid Scintillation Counting with Pulse-Shape Discrimination," Health Physics, 28: 5-11 (January 1975).

Nickles, R. J. and others. "A Flow-Through Detector for Nano-Curie Activities Encountered in HPLC Analysis of Pet Tracer Metabolites," IEEE Transactions on Nuclear Science, Vol 39, No 6: 2316-2321 (December 1992).

Nogues, J. L. and others. "Fast, Radiation-Hard Scintillating Detector: A Potential Application for Sol-Gel Glass," Journal of the American Ceramics Society, Vol 71, No 12, 1159-1163 (1988).

Omori, M. "Very Low Level α-particle Detection By Means of Pulse Shape Discrimination," Nuclear Instruments and Methods in Physics Research A, 337: 116-121 (1993).

Packard Instrument Co. "Material Safety Data Sheet," for Ultima Gold, 1990

Packard Instrument Co. Tri-Carb Series Liquid Scintillation Analyzers: Operation Manual. Meriden, CT: Packard Instrument Company, undated.

Peng, C. T., Horrocks, D. L. and Alpen, E. L. Liquid Scintillation Counting: Recent Applications and Development. Volume 1 and 2. New York: Academic Press, 1980.

Pope, Edward J. A. "Fluorescence Behavior of Organic Dyes, Europium, and Uranium in Sol-Gel Microspheres," Proceedings of SPIE - The International Society for Optical Engineering: Volume 1758: Sol-Gel Optics II: 360-371 (1992)

Prichard, H. M. and Cox, A. "Liquid Scintillation Screening Method for Isotopic Uranium in Drinking Water," in Liquid Scintillation Counting and Organic Scintillators. Ed. Harley Ross and others. Chelsea, MI: Lewis Publishers, 1991.

Ross, Harley H. "Photon Scattering Effects in Heterogeneous Scintillator Systems," in Liquid Scintillation Counting and Organic Scintillators. Ed. Harley Ross and others. Chelsea, MI: Lewis Publishers, 1991.

Ross, Harley H., Noakes, J. E. and Spaulding, J. D. Liquid Scintillation Counting and Organic Scintillators. Chelsea, MI: Lewis Publishers, 1991.

Rytz, A. "Alpha Energies and Intensities," Atomic Data and Nuclear Data Tables, Vol 47, No 2: 206-230 (March 1991)

Sowby, F. D. Annals of the ICRP, Pub 38: Radionuclide Transformations. Energy and Intensity of Emissions. New York: Pergamon Press (1983).

Walker, F. W., Parrington, J. R. and Feiner, F. Nuclides and Isotopes, 14th Ed. San Jose: General Electric Company, 1989.

Ward, Dann C. and Borak, T. B. "Determination of Time-Varying ^{222}Rn Concentrations Using Flow-Through Scintillation Flasks," Health Physics, Vol 61, No 6: 799-807 (December 1991).

West, Jon K., Kunetz, J. M., Araujo, F. G., and Hench, L. L. "Stability of Porous Sol-Gel Silica to Water Diffusion: Experimental and Theoretical Analysis," unpublished paper, 1994.

Vita

Captain Martin E. Keillor was born on 14 October 1963 in Stockton, California. He graduated from North Salem High School in Salem, Oregon in 1981 and attended Oregon State University, graduating with a Bachelor of Science in Engineering Physics in May 1985. He entered Officer's Training School in the Fall of 1986 and was commissioned as a 2nd Lieutenant in the USAF on 12 December 1986. His first duty assignment was as a student in the Basic Meteorology Program at Texas A&M University, which he completed with a 4.0 Grade Point Average. During 1988 and 1989, he served as Wing Weather Officer to the 352 Bombardment Wing and the 321 Strategic Missile Wing at Grand Forks AFB, North Dakota. He was then reassigned to Headquarters, 4th Weather Wing at Peterson AFB, Colorado, where he was selected to provide staff weather support to Headquarters, United States Space Command (USSPACECOM) and Headquarters, North American Aerospace Defense Command (NORAD). Upon the inactivation of 4th Weather Wing, he was reassigned to Headquarters, Air Force Space Command (AFSPACECOM) where he continued to provide staff weather support to USSPACECOM and NORAD until entering the School of Engineering, Air Force Institute of Technology, in June, 1993.

Permanent Address: c/o George W. Keillor
6091 Ogle Rd S.E.
Salem, Oregon 97301

REPORT DOCUMENTATION PAGE

Form Approved
OMB No. 0704-0188

1. AGENCY USE ONLY *(Leave blank)*	2. REPORT DATE	3. REPORT TYPE AND DATES COVERED
	December 1994	Master's Thesis

4. TITLE AND SUBTITLE
DETECTING ALPHA PARTICLES THROUGH SCINTILLATION IN POROUS MATERIALS

5. FUNDING NUMBERS

6. AUTHOR(S)
Martin Eugene Keillor
Captain, United States Air Force

7. PERFORMING ORGANIZATION NAME(S) AND ADDRESS(ES)
Air Force Institute of Technology
2750 P Street
WPAFB OH 45433-6583

8. PERFORMING ORGANIZATION REPORT NUMBER
AFIT/GAP/ENP/94D-05

9. SPONSORING / MONITORING AGENCY NAME(S) AND ADDRESS(ES)
N/A

10. SPONSORING / MONITORING AGENCY REPORT NUMBER

11. SUPPLEMENTARY NOTES

12a. DISTRIBUTION / AVAILABILITY STATEMENT
Approved for public release; distribution unlimited

12b. DISTRIBUTION CODE

13. ABSTRACT *(Maximum 200 words)*

This thesis presents the results of a preliminary study of parameters essential to the development of a scintillation flow-cell detector with improved characteristics over existing cells. Such a detector with better than 10% alpha energy resolution could provide *in situ* capability to detect and identify important alpha-emitting radionuclides in dilute aqueous solutions. Gel-silica is a potential candidate that may provide the needed improvement in resolution while maintaining 100% detection efficiency; however, gel-silica with useful light output is yet to be developed. As a step toward realizing the system described, the dependence of alpha detection efficiency and intrinsic energy resolution on the phase dimensions in heterogeneous scintillation detectors is examined. Two main areas of this research are: 1) computer modeling of the geometric detection efficiency and intrinsic energy resolution in porous glass scintillation detectors, and 2) experiments designed to test model predictions and provide data on the detection of alphas in porous glass structures. Experimental emphasis is on alpha detection in gel-silica filled with liquid scintillant. Results show that phase dimensions must be considered in constructing a flow-cell detector for alpha spectroscopy, and that the dimensions available in gel-silica provide for excellent intrinsic energy resolution, as well as 100% detection efficiency.

14. SUBJECT TERMS
Alpha Particle Detectors, Alpha Particle Spectroscopy, Scintillation Counters, Silica Gels, Silica Glass, Sol-Gel

15. NUMBER OF PAGES
113

16. PRICE CODE

17. SECURITY CLASSIFICATION OF REPORT	18. SECURITY CLASSIFICATION OF THIS PAGE	19. SECURITY CLASSIFICATION OF ABSTRACT	20. LIMITATION OF ABSTRACT
UNCLASSIFIED	UNCLASSIFIED	UNCLASSIFIED	UL